Accepted Manuscript

Syntheses and photodynamic activity of some glucose-conjugated BODIPY dyes

Neelam Shivran, Mrityunjay Tyagi, Soumyaditya Mula, Pooja Gupta, Bhaskar Saha, Birija S. Patro, Subrata Chattopadhyay

PII: S0223-5234(16)30540-2

DOI: 10.1016/j.ejmech.2016.06.050

Reference: EJMECH 8711

To appear in: *European Journal of Medicinal Chemistry*

Received Date: 16 May 2016

Revised Date: 13 June 2016

Accepted Date: 28 June 2016

Please cite this article as: N. Shivran, M. Tyagi, S. Mula, P. Gupta, B. Saha, B.S. Patro, S. Chattopadhyay, Syntheses and photodynamic activity of some glucose-conjugated BODIPY dyes, *European Journal of Medicinal Chemistry* (2016), doi: 10.1016/j.ejmech.2016.06.050.

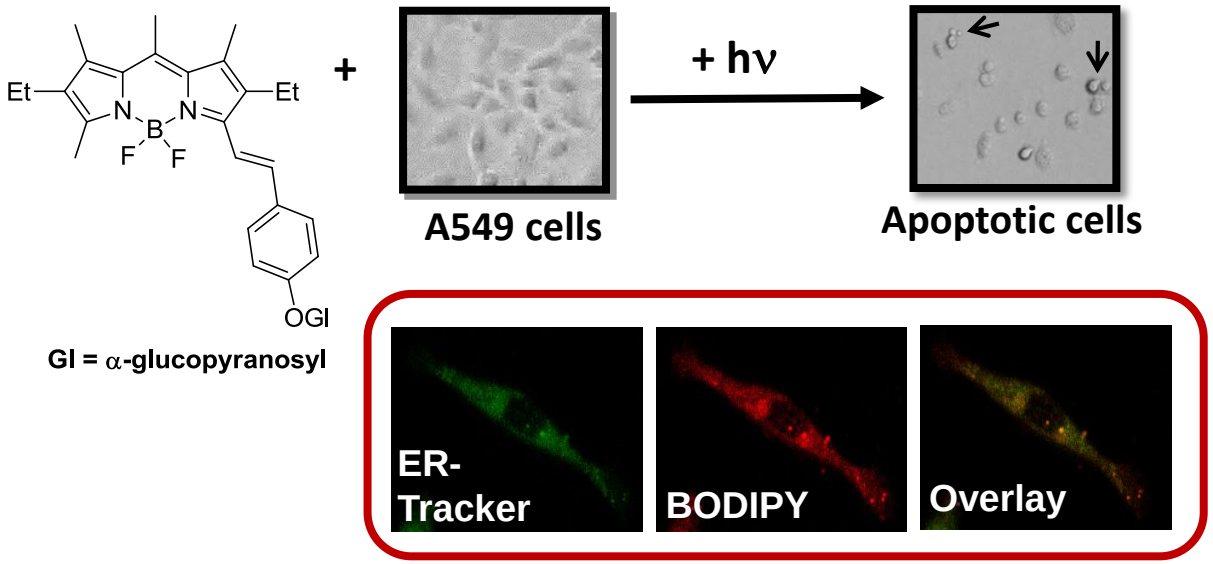

Gl = α-glucopyranosyl

The BODIPY-glucose conjugate localizes in endoplasmic reticulum to exert photodynamic effect on A549 cells.

Syntheses and photodynamic activity of some glucose-conjugated BODIPY dyes

Neelam Shivran,[#] Mrityunjay Tyagi,[#] Soumyaditya Mula,[#] Pooja Gupta, Bhaskar Saha, Birija S. Patro, and Subrata Chattopadhyay[*]

Bio-Organic Division, Bhabha Atomic Resesarch Centre, Mumbai 400 085, India

E. Mail: schatt@barc.gov.in

[#]Equal contributions

ABSTRACT- The syntheses of three water-soluble glucose-conjugated BODIPY dyes with different wavelength emissions and studies of their photodynamic therapeutic (PDT) action on human lung cancer A549 cell line are disclosed. Amongst the chosen compounds, the BODIPY dye **4** possessing a glycosylated styryl moiety at the C-3 position showed best PDT property against the A549 cell line. In particular, it induced reactive oxygen species-mediated caspase-8/ caspase-3-dependent apoptosis as revealed from the increased sub G1 cell population and changes in cell morphology. These results along with its localization in the endoplasmic reticulum, as revealed by confocal microscopy suggested that mitochondria may not be directly involved in the photo-cytotoxicity of **4**. Compound **4** did not induce any dark toxicity to the A549 cells, and was non-toxic to normal lung cells.

Keywords: apoptosis; BODIPY dyes; lung cancer; photodynamic property.

Highlights

- Formulation of a BODIPY dye, possessing a glycosylated styryl moiety at the C-3 position as a potent photodynamic agent.
- The BODIPY was phototoxic to human lung cancer A549 cell line, inducing caspase-8/ caspase-3-mediated apoptosis.
- The BODIPY was non-toxic to normal human lung cell lines, and was devoid of any dark cytoxicity.

1. Introduction

Photodynamic therapy (PDT) is a noninvasive treatment modality for a number of diseases including certain types of cancers and pre-cancerous inductions [1-3], age-related macular degeneration and actinic keratosis, localized infections, dermatological and cardiovascular illnesses and wound healing [4-7]. It relies on using a photosensitizer (PS), which on photo-excitation generates reactive oxygen species (ROS) in presence of oxygen to achieve selective irreversible cell killing. It is particularly promising in the treatment of multidrug-resistant (MDR) tumors, as both PS and light can be effectively localized in the tumor [8]. Evidently the chosen PS plays a key role in the outcome of the PDT. Some of the desirable attributes of the PS are its (i) ability to generate ROS, (ii) cellular internalization and biodistribution, and (iii) long wavelength (preferably in the red and/ or near IR regions) emission because of its better tissue permeability and cellular non-toxicity [9]. Long wavelength light is preferred for living subjects because it causes less photo damage to cells, and penetrates tissues better, while the higher wavelength light is absorbed by the tissues and is converted to heat energy.

Selective destruction of malignant cells sparing the normal tissues is another important issue in PDT. To a certain extent this is achieved by targeted light delivery to the tumor site, and can be improved further by conjugating the PSs with low molecular weight molecules that are better recognized by some of the overexpressed specific receptors in tumor cells [10,11]. The biodistribution and cellular uptake of the PS depends on the balance between its hydrophilicity and lipophilicity, as too high lipophilicity would hamper their transport through blood vessel, while a high hydrophilicity would impede its cell membrane penetration. Despite offering an alternative or complement to conventional therapies [12-14], the clinical use of PDT is restricted due to non-availability of an ideal PS. A few functionalized porphyrins, currently approved for clinical applications are not ideal PDT

drugs due to their low extinction coefficients in the therapeutic window (650–800 nm), and low absorptivity in mammalian tissues [15]. Therefore, there is a significant impetus to develop novel and more efficient sensitizers for use in PDT.

The dipyrromethene-BF_2 (4,4-difluoro-4-bora-3*a*,4*a*-diaza-*s*-indacene, BODIPY) fluorophores have gained importance for diverse applications due to their advantageous photo-physical properties including sharp absorption/ emission bands, high absorption coefficients and excellent fluorescence quantum yields that are relatively insensitive to changes in the local environment [16]. Most of these dyes have several characteristics of ideal PDT agents such as low dark cellular toxicity, good cellular uptake, high extinction coefficients, and low quantum yields for photobleaching. The BODIPYs are easy to synthesize, and most importantly, are amenable to extensive synthetic modifications that can help in tuning their florescence maxima and efficiency as well as ability to generate ROS. In view of these, development of BODIPY-based PDT agents continues to be an area of intense research, which has been elegantly reviewed [17,18]. Given that the BODIPYs are lipophilic, attachment of hydrophilic entities such as polyethylene glycol chains and carbohydrates to the BODIPY core might be useful in designing targeted probes for diagnosis as well as PDT agents. The PSs with sugar moieties are of great importance because sugar increases water solubility, membrane interaction and specific affinity for malignant tumors [19]. Carbohydrate-functionalized macromolecules have shown promise in photodynamic therapy and in vivo optical imaging due to their enhanced interactions with tumor cell receptors via carbohydrate-mediated cell recognition processes, and increased cellular uptake and solubility, without significant alterations of the physicochemical and photophysical properties [20,21]. Earlier, BODIPYs containing various hydrophilic groups have been used as imaging probes [22-24], and PDT agents [25-27]. Recently, cell internalization of some BODIPY-based fluorescent dyes bearing carbohydrate residues have

been studied by fluorescence microscopy [28,29], while synthesis and photophysical properties of some BODIPY-conjugated iminosugar clusters [30] as well as of lactosylceramide [31] have also been reported. In another study, some BODIPYs were grafted on a carbohydrate platform to synthesize artificial light-harvesting antenna [32]. In all these cases, the sugar moieties were attached to the dipyrrin carbon framework of the BODIPY fluorophore. In a significant departure from these methods, an interesting synthetic route for the direct attachment of the sugar moiety at the boron atom of the BODIPY fluorophore has been described very recently [33].

For the past few years, we are actively pursuing research in chemistry and applications of the BODIPYs [34-38]. The aim of the present study was to formulate some new glycosylated BODIPYs that can be easily synthesized, are bioavailable, and show good photosensitization to the target cells. Spin-coupling to heavy atoms (the ‘‘heavy atom effect’’) that ensures good intersystem crossing (ISC) rates is often used to augment generation of the cytotoxic ROS. However, the BODIPY derivatives are well-known to generate copious amount of ROS, especially $^1O_2$ that also leads to their oxidative degradation [34,37]. Hence, we did not address this issue. Moreover, the BODIPY PSs with heavy atoms, such as I, Br, Se, S etc. may offer increased dark toxicity, and altered bio-distribution as well as pharmacokinetics [39,40].

Recently, a novel synthesis of several iodinated BODIPY-compounds, containing a glucose moiety at the *meso*-appendage and oligo-ethylene glycol ethers at the 3,5-disubstituted 4-hydroxystyryl groups has been patented. Based on the MTT-based photocytoxicity data on MDA-MB-231 human breast cancer cell line, their potential application in targeted cancer therapy has been proposed [41]. In another study, some elegantly designed BODIPY molecules showed target-selective PDT property [42]. However, this warranted adoption of a complex synthetic strategy. Instead, we synthesized

three glycoconjugated BODIPY dyes (**2**, **4** and **6**) and compared their photosensitization property with their non-glycoconjugated precursors, **1**, **3** and **5** on the human lung carcinoma A549 cell line. The commercially available BODIPY dye (**PM567**) was used as a reference dye. The chemical structures of test samples are shown in Figure 1. In this panel of molecules, we have incorporated a phenol moiety at the *meso*- or the pyrrole 3/5 positions of the BODIPY core for the attachment of the glucose moiety. Introduction of the styryl phenol moiety at the 3/5-position of the pyrrole ring also helped in synthesizing the dyes with red-shifted emissions. Relevant physico-chemical parameters, such as absorbance/ emission profiles, fluorescent quantum yields, and DNA binding characteristics of the dyes were also determined. Next, the PDT property of the test compounds was examined and the results mechanistically rationalized by assessing some biochemical parameters. We chose the human lung cancer A549 cell line for the present studies as lung cancer is one of the most common malignancy in humans and has become the leading cause of death. Despite the rapid progress of surgery, radiotherapy, chemotherapy, and biotherapy, the long-term survival rate of patients with lung cancer remains poor, and new therapeutic strategies are urgently needed [43,44]. Since early lung cancer detection is now becoming feasible, PDT may be applied to treat early stage lung carcinoma. Several clinical trials have established its efficacy with superficial small tumors, while its use as a preoperative measure may reduce tumor burden and the degree of surgery for larger tumors [45].

2. Results and discussion

2.1 Synthesis

The syntheses of the parent BODIPYs were straightforward. Thus, kryptopyrrole **7** was condensed with benzaldehyde or 4-hydroxybenzaldehyde in presence of *para*-toluene sulphonic acid (PTS) to obtain compounds **8** [34] and **1** respectively. The reaction is usually carried out in CH_2Cl_2 when the BODIPYs are obtained in moderate yields with most of the

aromatic aldehydes [34]. During the synthesis of **1**, it was found that the reaction was very slow and produced a dark brown mixture resulting in poor yield of the isolated product. However, minor modifications of the reaction conditions such as use of THF as the solvent and addition of DDQ at 0 °C improved the yield of **1**, as the reaction was clean and the product isolation easy. The BODIPY dyes containing C-3/5-CH_3 substituted pyrrole rings undergo the base-catalyzed Knoevenagel-type condensations with various aryl aldehydes. This strategy has been extensively used to synthesize BODIPY derivatives with red-shifted fluorescence [46,47]. Hence, for the present synthesis, the dyes, **PM567** and **8** were individually subjected to condensation with 1.0 equivalent of 4-hydroxybenzaldehyde in the presence of piperidine and acetic acid to obtain the monostyryl derivatives **3** and **5** respectively (**Scheme 1.**) along with trace (5-7%) amounts of the corresponding distyryl products, which were discarded by column chromatography.

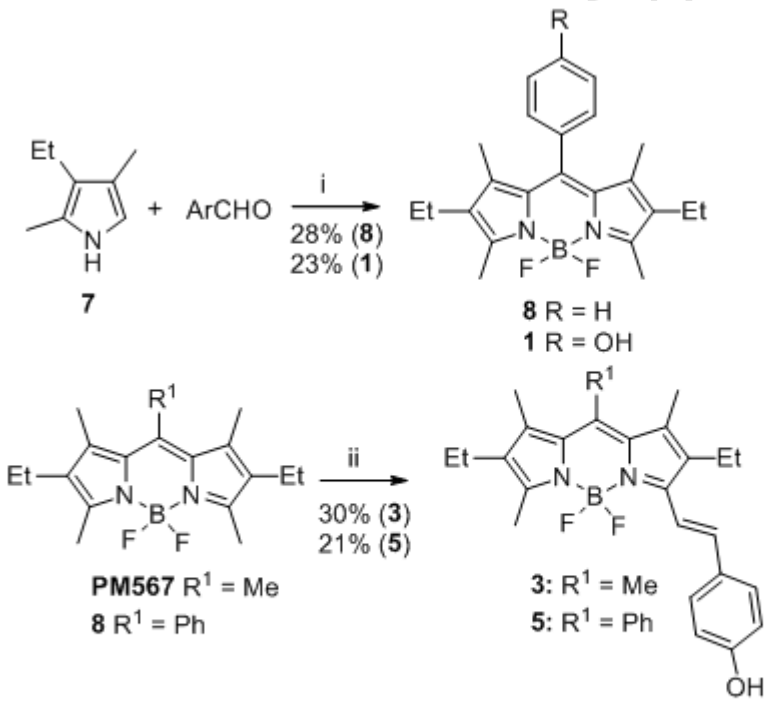

i) PTS/CH_2Cl_2 (for benzaldehyde) or THF (for 4-hydroxybenzaldehyde)/25 °C /24 h; DDQ/4 h; Et_3N/1 h; $BF_3.Et_2O$/25 °C/12 h, ii) piperidine/ AcOH/toluene/Δ.

Scheme 1.

The required glycosylation of the phenolic functionality in **1** and **3** was achieved using glucose pentaacetate as the glycosyl donor in presence of $BF_3.Et_2O$ catalyst in CH_2Cl_2 to furnish **9** and **10** respectively (**Scheme 2.**). However, the same strategy with **5** led to its considerable degradation, and furnished the required glycoside **12** in very low yield. Glycosylation of **5** was subsequently achieved by the improved classical Konigs-Knorr method, involving a base (K_2CO_3)-catalyzed reaction of **5** with 2,3,4,6-tera-O-acetyl-alpha-D-glucopyranosyl bromide (**11)** in 1:1 $H_2O/CHCl_3$ to obtain **12** [48]. The glucosyl donor **11** was synthesized from glucose pentaacetate by a tandem chemo-selective deacetylation of its anomeric acetyl group and bromination with HBr-HOAc. It is well established that the configuration of the anomeric sugar carbons remains unaffected during glycosylation [49]. Finally compounds **9**, **10** and **12** were deacetylated with NaOMe in MeOH to obtain the target BODIPYs **2**, **4** and **6** respectively.

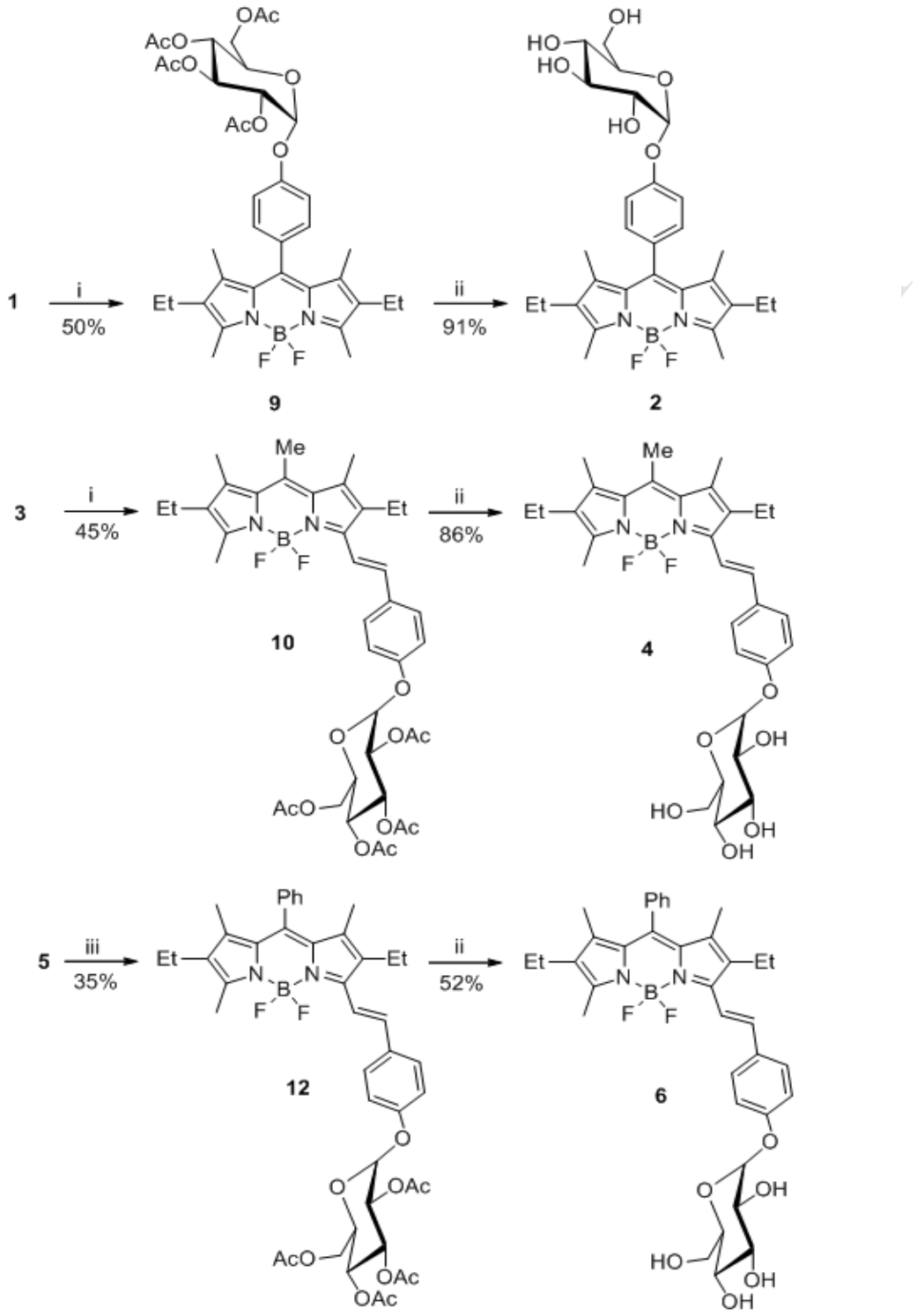

i) Glucose pentaacetate/$BF_3.Et_2O/CH_2Cl_2$/reflux/3 h, ii) NaOMe/MeOH/25 ^oC/1 h,
iii) 2-Bromoglucose tetraacetate (**11**)/K_2CO_3/Bu_4NBr/1:1 H_2O-CH_2Cl_2/40 to 60 ^oC/6 h.

Scheme 2.

2.2 Photophysical characteristics

The photophysical (absorption and fluorescence) data of the BODIPY-*O*-glycosides **2**, **4**, and **6** in ethanol are summarized in Table 1. All the compounds exhibited typical spectral characteristics of the BODIPY core with a narrow $S_0 \rightarrow S_1$ absorption band with high molar extinction coefficients, intense fluorescence emissions and small Stokes' shifts (Figure SL1). The absorption and emission spectra were almost mirror images of each other, indicating that the emitting and absorbing species are similar. Compared to the non-styrylated BODIPY **2**, introduction of a styryl group as in **4** and **6** induced significant bathochromic shifts in the absorption (51-63 nm) and emission (50-55 nm) maxima. The lower fluorescence quantum yields of **4** and **6** indicated significant nonradiative energy loss due to rotation around the C-Ar bonds [50]. Because the BODIPYs do not show solvatochromism, the photophysical measurements were made in ethanol only.

Table 1. Photophysical parameters of the dyes **2**, **4** and **6** in ethanol.

Dye	λ_{abs} (nm)[a]	ε_{max} (10^4 $M^{-1}cm^{-1}$)[b]	$\lambda_{em\ (nm)}$[c]	Φ_{fl}[d]
2	522.6	8.3	540	0.84[e]
4	573.8	8.2	590	0.60
6	586.0	8.0	595	0.52

[a]Error: ± 0.2 nm. [b]Extinction coefficients at the λ_{max}. [c]Error: ± 1.0 nm. [d]The fluorescence quantum yields of the dyes **4** and **6** are relative to that of the dye rhodamine 101 (Φ_{fl} = 1.0 in EtOH). [e]The fluorescence quantum yields of **2** is relative to that of PM567 (Φ_{fl} = 0.84 in EtOH).

2.3 DNA binding characteristics

By and large, the PSs exert their photo-dynamic action by generating $^1O_2$, which has a short lifetime (ca. 2.0 μs) with a low apparent diffusion coefficient (4×10^6 cm^2 s), and thus, a very limited sphere of activity (about 150 nm in radius) in biological systems. This

implies that binding to DNA is a desirable characteristic of the PDT agents, because the generated $^1O_2$ can induce DNA damage. Hence, the strong absorption bands of **2** and **4** at 522.6 nm and 573.8 nm respectively were conveniently used to determine their DNA binding characteristics by spectrophotometric titrations. Incremental addition of double stranded calf thymus (CT)-DNA (0–200 µM DNA base pair) to a fixed concentration of **2** (20 µM) and **4** (50 µM) led to gradual reductions in the intensities of their respective absorption maxima (Figures SL2A and SL2B), confirming binding with DNA. Based on the site-exclusion model [51], the equilibrium binding constants (K) in respective cases were derived by quantitative analysis of the UV–visible data (Figures SL3A and SL3B). The moderate K-values of 3.4×10^4 M^{-1} and 1.8×10^4 M^{-1} respectively for **2** and **4** suggested an ionic binding, because the DNA-intercalators generally show higher binding constants ~10^5 - 10^7 M^{-1}. Moreover, well-known DNA intercalators such as coralyne produce new species on binding with DNA [52]. Presently no additional absorption peak was observed on titration of DNA with the dyes **2** and **4**. The linear fits in regression analyses also indicated a single mode binding of the dyes with DNA. We did not determine the DNA binding constants of the other test samples based on the biological results (*vide infra*).

2.4 Biology

For the biological studies, the *in vitro* photodynamic activities of **1**-**6** and the commercial dye **PM567** (as a reference molecule) were assessed by the MTT assay using the highly invasive and metastatic human lung cancer A549 cell line. All the biological experiments were carried out using the vehicle (≤ 0.1% DMSO in DMEM) that was non-toxic to the cells. Throughout the manuscript, control refers to the photo-exposed cells in vehicle. Initially the cells were photo-exposed (irradiance: 0.77 mW/cm^2) for different periods (0.5-4 h) in the presence of fixed concentrations (500, 1000 and 5000 nM) of **1**-**6** and the growth inhibition was assessed by the MTT assay at 24 h following photo-exposure.

At all the chosen concentrations of the compounds, photo-exposure time-dependently reduced the viabilities of the A549 cells, with respect to the corresponding controls (Figure SL4). However, the growth inhibitions at 1 and 2 h were not significantly different. Hence, a 80 min photo-exposure was chosen for the elaborate dose-dependent MTT assays with the compounds **1**-**6** and **PM567**. Based on these results (Figure 2A), the growth inhibitory IC_{50} values, defined as the concentrations of the dyes required to kill 50% of the cells were calculated and are shown in Table 2. In absence of light, none of the test compounds (up to 200 μM) showed any toxicity to the A549 cells, as revealed by the MTT assay results at 24 h (data not shown). This excluded the possibility of any dark toxicity of the compounds. Likewise, photo-exposure (up to 4 h) alone was non-toxic to the cells (Figure SL5), establishing that light alone or temperature of the irradiating apparatus was not responsible for the observed results. We used a long CFL tube (2 ft) along with a reflector for an uniform photo-exposure. The irradiance, measured at 8-10 positions of the plates showed a marginal (~2%) variation, confirming homogeneity of irradiation all over the plates.

The relative potency of the test compounds was **1**>**6~4**>**3~5~PM567**>>**2**. The results with the glycosylated dyes **4** and **6** *vis-à-vis* the corresponding parent dyes **3** and **5** clearly revealed that glycosylation improved the potency of the styryl BODIPYs. But shifting the emission maxima to longer wavelengths had insignificant effect on the PDT activity, as is evident from the similar IC_{50} (~6.5 μM) values of the non-conjugated **PM567** dye and the conjugated styryl BODIPYs **3** and **5**. Earlier we have shown that presence of a bulky *meso*-substitution such as an aryl group in the BODIPYs reduce their $^1O_2$ generating ability [34]. It is possible that the large glycosylated phenol substitution at the *meso*-position of compound **2** does not allow significant $^1O_2$ generation, explaining its poorer PDT activity compared to that of its non-glycosylated precursor **1**. This is consistent with a previous report, wherein the *in vitro* and *in vivo* photosensitizing property of some lactose-conjugated porphyrinoids

depended on the site of the sugar in the PSs [53]. It is worth noting that earlier, compound **1** showed impressive PDT property against the human colon carcinoma cell line HCT116 [54].

Table 2. Comparative cytotoxicities of the chosen BODIPYs against A549 human lung cancer cells[a]

Test compounds	IC_{50} (μM)[a]
PM567	$6.8 \pm 1.8^{*}$
1	$2.1 \pm 0.6^{*}$
2	> 10
3	$6.5 \pm 2.1^{*}$
4	$2.7 \pm 0.8^{**}$
5	$6.4 \pm 2.0^{*}$
6	$2.5 \pm 1.1^{**}$

[a]The IC_{50} values were calculated using the MTT data shown in Figure 2A. The experiments were repeated three times with similar results. All determinations were made in four replicates, and the values are means ± S. E. M. $^{*}P<0.001$ compared to **2**, $^{**}P<0.001$ compared to the corresponding non-glycosylated BODIPYs.

Despite showing the best result amongst the test compounds, the photo-cytotoxicity of **1** was primarily due to necrosis as revealed by phase contrast microscopy of the trypan blue-stained cells. Photo-exposure of the cells, treated with **1**, but not with **4** and **6** showed significant accumulation of the blue dye in the cells within 2 h (Figure 2B). This indicated extensive membrane damage induced by **1**, leading to necrosis. Hence we excluded compound **1** for further studies. Although both **4** and **6** showed similar potency, compound **4** was easily accessible from commercially available materials. Hence, the subsequent

mechanistic studies were carried out with the BODIPY dye **4**. However, the cellular uptake and distribution studies were carried out with all the chosen compounds **1-6** and PM567.

Apoptosis induction is a preferred mode of killing the cancer cells due to less side effects and immune reactions [55]. In the present study, apoptosis induction by **4** was confirmed by following several apoptosis-specific parameters: (i) sub-G1 cell population, (ii) cell morphology, and (iii) cell survival analyses in the presence of a pan-caspase (Z-VAD-FMK) as well as three specific caspases inhibitors. At a 30 min photo-exposure, compound **4** (5-50 μM) increased the sub-G1 cell population by ~2.8-3.3 folds, compared to control. The effect was more severe with a 80 min photo-exposure, when the sub-G1 cell population increased by 5-6 folds (Figures 3A and 3B). There was no alteration in the sub-G1 population in the cells treated with **4** (up to 50 μM) in the absence of any photo-exposure. This clearly established the lack of dark toxicity of **4** against the A549 cells.

The phase contrast microscopy, performed to examine the effect of compound **4** (up to 2.5 μM) in conjunction with a 80 min photo-exposure showed obvious and significant morphological changes in the A549 cells. At 24 h after the treatment, the cells showed marked changes in the cell outline, with irregular disruptions in the optical diffraction halo, and the effect was concentration dependent. The number of shrinking cells or cells with blebbing membranes was notably increased in the **4**-treated cells than in the control (Figure 3C). There were number of floating cells without any adhering ability in the treated group than in the controls.

Apoptosis can be induced by the ligation of plasma membrane death receptors, which stimulate the ‘extrinsic’ pathway, or by perturbation of intracellular homeostasis, the ‘intrinsic’ pathway [56,57]. The extrinsic pathway is initiated by the binding of a member of the tumor necrosis-factor (TNF)-family of death-receptor ligands to their cognate receptors (TNFR or Fas). The oligomerized receptors subsequently recruit adaptor protein (TRADD or

FADD), which in turn, recruits pro-caspase-8 and/or pro-caspase-10 to form the death inducing signaling complex (DISC). As a part of the DISC, pro-caspase-8 becomes autocatalytically activated to cleave the effector pro-caspase-3/7. The intrinsic pathway is linked primarily to mitochondrial changes, directly inducing the release of cytochrome c into the cytosol and apoptosome complex formation with activation of caspase-9. Both pathways converge on caspase-3 activation, resulting in nuclear degradation and changes in cellular morphology. In our results, treatment of the A549 cells with **4** (2.5 μM) followed by a 80 min photo-exposure stimulated the activities of caspase-3 (~2.9 fold) and caspase-8 (~6.2 fold) without any increase in the caspase-9 activity, compared to the untreated control cells (Figure 4A). The specific inhibitors (each 20 μM) for caspase-3 (Z-DEVD-FMK) and caspase-8 (Z-IETD-FMK) abrogated such activation of the respective caspases by 46.7% and 48.6%. Expectedly, the caspase-9 specific inhibitor (Z-LEHD-FMK, 20 μM) was ineffective (data not shown). To further confirm the involvement of caspase-8/caspase-3 pathway in the photo-toxicity of **4** in the A549 cells, we assessed the cell survival (at 24 h) in the absence and presence of the above caspase-specific inhibitors as well as the pan-caspase inhibitor (each, 20 μM). Pre-incubation of the cells with the caspase-8, caspase-3 as well as the pan-caspase inhibitors increased their viability by 50.6%, 36.5% and 77.2% respectively, compared to the only compound **4**-treated and 80-min photo-exposed cells. However, the caspase-9 inhibitor did not show significant effect on cell survival (Figure 4B). None of the above inhibitors, on their own altered the activities of the caspases and the cell survival in absence of **4**. Our immunoblots (Figure 4C) also showed a time-dependent reduction in the pro-caspase-3 levels in the compound **4** plus 80-min photo-exposed cells compared to the control cells. Taken together, these results suggested involvement of the extrinsic apoptotic pathway in the photo-toxicity of **4** to the A549 cells, where caspase-8/caspase-3 activation plays a major role. No caspase-3 activation was noticed by treating the cells with **4** alone (data not shown). Current

evidence suggests that the mitochondrial pathway is most common in PDT-induced apoptosis in cells. However, the caspase-8-dependent pathways may also be important, when the dominant pathway is suppressed [58].

Due to their higher metabolic rates, cancer cells are generally under more oxidative stress than the normal cells [59]. PDT causes photooxidative damage to proteins and lipids that reside within a few nanometers of the PSs binding sites [58]. There is strong evidence that ROS can induce the apoptotic process [60]. Hence, we examined if ROS generation is responsible for the photo-toxicity of **4**, by carrying out the sub-G_1 cell population assay in the absence and presence of β-carotene (a specific $^1O_2$-inhibitor) [61] and *N*-acetyl cysteine (NAC, a cell-permeable antioxidant). In addition, the cell survival assay was also carried out under similar conditions in the presence of increasing concentrations of β-carotene. As revealed from the results (Figures 5A and 5B), incubation of the cells with β-carotene (50 and 100 μM) or NAC (5 mM) along with **4** (2.5 μm) followed by a 80 min photo-exposure reduced the sub-G_1 cell population by 24.2%, 36.7% and 32.4% respectively, compared to the only **4**-treated and 80-min photo-exposed cells. In the MTT assay, β-carotene dose-dependently reduced the photo-toxicity of **4**, offering 46.5% protection at a concentration of 50 μm. The above results confirmed that the intracellular ROS, especially $^1O_2$ was responsible for the PDT property of **4** in the A549 cells.

Photodynamic efficacy is principally determined by the subcellular localization of a PS that governs the primary site of photodamage [62]. Some PSs show a broad distribution, while some may localize more specifically. Hence, fluorescence microscopic studies were carried out to investigate the cellular uptake and localization of the test compounds. All the BODIPY dyes exhibited cytoplasmic localization in the A549 cells as revealed from the red fluorescence (Figures 6A and 6B, middle panel). The images of the cells, stained with the nucleus specific dye, Hoechst-33342 are shown in the left panel of the same figures. The

merged images (right panel) clearly revealed that the intra-cellular accumulation of all the dyes was outside the nucleus. Compared to the other dyes, PM567 showed lower fluorescence, indicating its less cellular uptake. Also, the patchy fluorescence in the cells, stained with **1** indicated its non-uniform presence in the cytoplasm with higher accumulation near the membrane. This may also account for its observed necrotic property. The other dyes had uniform florescence all over the cytoplasm of the cells.

The subcellular localization of **4** was ascertained by confocal microscopy using dual staining with **4** (100 nm) followed by the organelle-specific fluorescence probes *viz*. Lyso-Tracker Green, Mito-Tracker Green or ER-Tracker Green. The clinically used PS, photofrin has been shown to concentrate into plasma membranes or cytoplasm upon brief incubation, and in the Golgi complex or ER upon prolonged incubation [63,64]. In our experiments, fast cellular internalization of **4** was noticed within a few minutes. Although we have incubated the cells with **4** up to 4 h, no significant change in its distribution in the subcellular compartments was noticed by varying the incubation time points (0.5, 1, 2 and 4 h). Presently, the confocal images for 1 h-incubation with **4** is shown in Figure 7, as the same incubation time was used for the experiments, prior to photo-exposure. The left and middle panels show the images of the cells, loaded with the respective fluorescence probes and compound **4**, while their superimpositions are shown in the right panel. There was an almost identical overlap of the images of the cells loaded with compound **4** and the ER-Tracker, indicating that ER is the preferential accumulation site of compound **4**. In comparison, colocalization of compound **4** was only partial with Mito-Tracker and very less with Lyso-Tracker. This result is consistent with the fact that compound **4** did not activate caspases-9 to induce mitochondrial apoptosis in the A549 cells. Several observations have indicated that the PSs that localize within mitochondria or ER promote apoptosis. Since compound **4** did not accumulate in the plasma membrane or lysosomes, it did not promote cell necrosis

[58,65]. It is also very unlikely to directly damage DNA, as the nucleus remained free of compound **4**. No significant alteration in the morphology was observed on incubating the cells with **4** up to 4 h in dark (data not shown).

Activation of the caspases is perhaps the most well characterized apoptotic cascade, and caspase-3 activation is a landmark event in apoptosis [66]. Our results showed activation of caspase-8 and caspase-3 in the A549 cells by **4** under photo-exposure leading to increased sub-G1 cell population that was abrogated by the specific as well as pan-caspase inhibitors. It has been reported that procaspase-3 localizes in the cytoplasm and that caspase-3 activation is initiated in the cytosol, followed by its redistribution to the nuclear compartment [67,68]. Because compound **4** also accumulates in the cytoplasm of the cells, it is expected to induce the caspase-3-mediated apoptosis. Structurally, the BODIPYs constitute half of the porphyrins that are known to be specifically accumulated in tumor cells. Hence, we anticipated good tumor-selectivity of the BODIPYs. This was confirmed by the MTT assay using normal human lung cell lines, WI-38 and L132. Compound **4** (50 μM) induced only 5-7% cytotoxicity in these cells under photo-exposure.

The main objective for adding a sugar moiety to the BODIPY scaffold was to ensure preferential accumulation and/or retention in cancer *vis-à-vis* normal cells. To probe these, we studied the uptake and retention of the dyes **3** and **4** (2.5 μM each) in A549 lung cancer cell line from their fluorescence, using flow cytometry. The dye **4** is the glycosylated derivative of dye **3**. The relative amounts of the dyes inside the cells were quantified in terms of the mean fluorescence intensity (MFI) in the red (FL3) channel [69]. A higher uptake and longer retention of the dye **4** in the cells was observed, compared to **3** (Table 3). This may be one of the reasons of its enhanced capacity in inducing death in the cancer cells *vis-à-vis* **3**. To rationalize the selective photocytotoxicity of **4** to cancer cells over normal cells, we also carried out similar experiments with L132 and A549 cell lines. The initial uptake (at 2 h) of **4**

by A549 cells was significantly higher than by L132 cells. Since the internalization of **4** was very fast and the experiments were carried out within 80 min, its selective photocytotoxicity to the cancer cells compared to normal cells is expected. The higher uptake of **4** by the A549 cells compared to the L132 cells may be due the altered expression levels of many of the plasma membrane proteins in the cancer cells *vis-à-vis* normal cells [70].

Table 3. Comparative uptake and retention of **3** and **4** in human lung cancer A549 cells and of **4** in normal (L132) *vs* cancer (A549) human lung cells[a]

Sample	MFI in A549 cell line		MFI of compound **4**	
	Comp. **3**	Comp. **4**	L132	A549
Control	2.4±1.1		4.6±1.2	5.4±1.5
2 h	88.0±6.8*	98.5±7.2$^{*,\#}$	63.5±4.5*	95.3±6.3$^{*,\tau}$
4 h	53.7±6.2*	68.9±6.3$^{\#}$	56.8±5.4*	66.2±4.6$^{*,\$}$
8 h	43.9±5.5*	58.4±6.1$^{\#}$	49.5±5.8*	49.4±6.0*
16 h	40.9±5.9*	52.5±5.8$^{\#}$	41.5±4.2*	41.6±3.7*
24 h	38.4±4.8*	46.7±5.9$^{\#}$		

[a]The A549 cells were treated with **3** or **4** (2.5 μM) for different periods and the intracellular concentrations of the compounds were analyzed by flow cytometry from the red florescence (FL3 channel). The data are presented in terms of MFI in arbitrary units. Similar experiments were also carried out with **4** (2.5 μM) using A549 and L132 cells. The experiments were repeated three times with similar results. All determinations were made in four replicates, and the values are means ± S. E. M. $^{*}p<0.001$ compared to control cells, $^{\#}p<0.05$ compared to the **3**-treated cells; $^{\$}p<0.05$, $^{\tau}p<0.01$ compared to the L132 cells.

We adopted indirect methods to ascertain apoptosis induction and ROS production by the dye **4** under photo-exposure. This is because of the overlapping fluorescence spectra of the respective probes (FITC tagged annexin-V and DCFDA respectively) with that of **4** at its IC_{50} concentration. For the same reason, we did not measure the amount of $^1O_2$ produced by it, by the 1,3-diphenylisobenzofuran bleaching method [71]. Nevertheless, we have provided multiple lines of evidence to ascertain that the photo-toxicity of **4** to the A549 cells follows apoptosis by assessing the sub G1 cell population, cell morphology and identifying the involvement of the caspase-mediated pathway. We have also used two intracellular ROS inhibitors, including β-carotene, a well-known $^1O_2$-specific inhibitor (at different concentrations) to provide ample evidence of the involvement of $^1O_2$ in the process.

3. Conclusions

Overall, we developed a new water-soluble BODIPY dye **4** possessing a glycosylated styryl moiety at the C-3 position by a simple synthetic route. The dye **4** showed impressive photo-sensitization property against the human lung carcinoma (A549) cell line, inducing ROS-mediated apoptosis via the caspase-8/caspase-3-dependent extrinsic pathway. Its accumulation in cell cytoplasm matched with the localization site of procaspase-3 to ensure apoptosis without any necrosis. The dye **4** did not show any dark toxicity to human normal lung (WI-38 and L132) and cancer (A549) cell lines, and was non-toxic to the normal lung cells even on photo-exposure. Compared to dye **4**, some halogenated BODIPYs earlier showed lower IC_{50}-values in their photo-dynamic property [17,18]. However, their photo-toxicity against the non-targeted normal cells has not been verified. Considering their possible dark toxicity, increasing attention is being paid to develop halogen-free BODIPYs as PDT agents, and BODIPYs with extended conjugation have emerged as promising candidates [17,39,40]. However, it is difficult to synthesize these BODIPYs in sufficient amounts for their clinical applications. By contrast, dye **4** can be easily synthesized in an overall yield of

11.6% in 3-steps from the commercially available PM567 dye using inexpensive chemicals/reagents, is bioavailable, and shows selective photosensitization to the target cells.

4. Experimental Section

4.1 Synthesis

The syntheses of the target BODIPYs were achieved as shown in **Scheme 1** and **Scheme 2**. Detailed experimental procedures as well as the characterization data of the BODIPYs and the intermediates involved in the syntheses are provided in the supplementary material.

4.2 General Biology

Penicillin, streptomycin, 3-(4,5-dimethylthiazol-2-yl)-2,5-diphenyltetrazolium bromide (MTT), β-carotene, N-acetylcysteine (NAC), Triton X-100 (0.1%), Tween 20, propidium iodide (PI), phenylmethylsulfonyl fluoride (PMSF), aprotinin, leupeptin, sodium orthovanadate ($NaVO_4$), and rabbit polyclonal antibody to caspase-3, RNase were procured from Sigma chemicals (St. Luois, MO). Other chemicals used were: Dulbecco's modified Eagle's medium (DMEM), fetal bovine serum (FBS), trypan blue (Gibco Life Technologies, Carlsbad, CA), Hoechst 33342 (Molecular Probes, Inc., Eugene, OR), pan caspase inhibitor (Z-VAD-FMK), specific inhibitors of caspase-9 (Z-LEHD-FMK), caspase-3 (Z-DEVD-FMK) and caspase-8 (Z-IETD-FMK) (R&D Systems, Minneapolis, MN), and rabbit polyclonal antibody to β-actin (Abcam, Danvers, MA). Lumi-Light ^{PLUS} western blotting kit and cell death detection ^{PLUS} kit were procured from Roche Applied Science (Baden-Wurttemberg, Mannheim), while nitrocellulose membrane (BioTrace® NT) was from Pall Life Sciences (Easthills, NY).

4.2.1 Cell culture

The A549 cell line, procured from National Centre for Cell Science, Pune, India were cultured in DMEM medium, supplemented with 10% FBS, 100 U/mL penicillin and 100 μg/mL streptomycin. The cells were grown at 37 ^{o}C under an atmosphere of 5% CO_2.

4.2.2 Drugs preparation

Stock solutions (50 mM) of the test samples in DMSO were reconstituted in DMEM medium without any nutrient to attain the required doses of them for the MTT assay. For the other assays, the samples were prepared as above using 5 mM stock solutions of the respective compounds. The final DMSO concentration in all the samples was <0.1%.

4.2.3 Photo-exposure protocol

The cells were irradiated with white light from a CFL source (2 ft long, 20 W, Phillips), mounted on polished reflector unit. The distance between the light source and the surface of the irradiated solutions was ~5 cm. The irradiance on the plates was measured at 8-10 locations of the plates with a model LX-101A research light meter (Eztech Instruments, Nashua, NH, USA). The mean value was 0.77 mW/cm^2 (variation ~2%). The photo-irradiation unit was housed in the CO_2 atmosphere.

4.2.4 MTT assay

Viabilities of the control and treated cells were determined by the MTT reduction assay [72]. The A549 cells (1×10^4/well) were grown in 96-well plates in DMEM medium supplemented with 10% FBS at 37 °C in a 5% CO_2 atmosphere. Cells were plated overnight prior to any treatment. The unsynchronized cells were treated with vehicle (0.1% DMSO) or the compounds (each 500, 1000 and 5000 μM) for 1 h in serum-free medium, washed twice with phosphate-buffered saline (PBS), followed by photo-irradiation for different periods (0.5, 1, 2, and 4 h) at 37 °C in a 5% CO_2 atmosphere. The cells were subsequently incubated in a regular medium for 24 h, washed once with PBS, MTT solution (0.5 mg/mL, 100 μL) was added to each well and kept at 37 ^{o}C for 6 h. The formazan crystals in the viable cells

were solubilized with 0.01 N HCl (100 μL) containing 10% SDS and the absorbance at 550 nm read.

For determining the IC_{50}-values, the assay was carried out as above, using different concentrations of the compounds and a 80-min photo-exposure. Similar assays were also carried out by pre-incubating the cells with the specific and pan caspase inhibitors (each 20 μM) or increasing concentrations of β-carotene (0-100 μM) for 1 h prior to the addition of the test compound **4** (2.5 μM). The dark toxicities of the compounds were assessed at 48 h as above, omitting any photo-exposure.

4.2.5 Phase contrast microscopy

The A549 cells (1×10^5 cells/well) were cultured overnight on cover slips in 6-well plates. The cultures were incubated with vehicle (0.1% DMSO) or the dyes **1**, **4** and **6** (each 2.5 μM) for 1 h, followed by photo-irradiation for 80 min. After addition of serum, the cells were incubated for 2 h, washed twice with PBS, trypan blue (0.1% in PBS) added and incubated further for 5 min. The cells were washed once with PBS, mounted on glass slides, visualized, and representative fields of the cells were photographed using an Axioskop II Mot plus (Zeiss) microscope (40 × objective, 0.65 Ph2), fitted with a Axiocam MRc camera. Similar experiments were also carried out after treating the cells with different concentrations of **4** as above, and visualizing the cells after 24 h without trypan blue staining.

4.2.6 Flow cytometry

The hypodiploid DNA content were analyzed as a marker for apoptosis by flow cytometry, after staining with PI. The cells were incubated with **4** (0-50 μM) for 1 h, washed two times with PBS, DMEM (200 μL) added, and subsequently exposed to light for different time periods (30 and 80 min). After addition of serum, the cells were incubated for 24 h, washed once with cold PBS, incubated with PI (400 μg/mL) and RNAse A (200 μg/mL) in 1 mL hypotonic buffer (0.1% sodium citrate plus 0.1% Triton X-100) for 30 min at 37 ^{o}C, and

analyzed with a Partec CyFlow® Space flow cytometer using the FlowJo program. Cellular debris was excluded from the analyses by raising the forward scatter threshold, and the DNA content of the nuclei was registered on a logarithmic scale. At least 2×10^4 cells of each sample were analyzed. The cell number read by flow cytometry for every single sample was same, although the total areas under some curves look different. This is because of the normalization done by the software in the overlayed histograms. The normalization is required to avoid disproportionate heights of the histograms of different fluorescence intensities for the two overlaid samples, and is achieved by plotting "% of max" instead of "total cells counted or events taken" in the Y-axis [73]. The apoptotic nuclei appeared as broad hypodiploid DNA peaks. Similar experiments were also carried by treating the cells with NAC (5 mM) and β-carotene (50 and 100 μM) along with compound **4** (2.5 μM) and photo-exposure for 80 min.

For the dye retention studies, the A549 cells (1×10^5 per well), grown in 6 well plates as above were washed twice with PBS and treated with vehicle (0.1% DMSO) or the dyes, **3** and **4** (2.5 μM each) for 2 h in a serum-free medium. After washing twice with PBS, the cells were incubated in a regular medium at 37 °C in a 5% CO_2 atmosphere for different periods as described in the Table 3. The cells were trypsinized, washed with PBS and analyzed through flow cytometry. Similar experiments were also carried out using dye **4** and L132 cells. The data are presented in terms of MFI.

4.2.7 Fluorescence microscopy

A549 cells seeded in 6-well plates on coverslips were loaded with the BODIPY dyes (1 μM) for varying periods (0.25, 0.5, 1, 2 and 3 h) at 37 ºC, washed with PBS, subsequently stained with Hoechst 33342 (10 μM), washed once again with PBS, mounted with 70% glycerol, and analyzed under an Axioskop II Mot plus (Zeiss) microscope (40 × objective, 0.65 Ph2). Some adjustments to the stretch and tone of both blue and red images were made

while overlaying the images. This was done only for better contrast and to ensure that the blue color of the Hoechst-stained nucleus and red color of the dye are both visible.

4.2.8 Confocal microscopy

The overnight-seeded cells were washed twice with PBS, stained with dye **4** (100 nM for 2 h), washed again with PBS, and then stained with LysoTracker Green (500 nM), MitoTracker Green (100 nM), or ER-Tracker Green (500 nM). The cells were incubated for 30 min at 37 °C. In all cases, the cells were washed again with PBS before imaging through confocal microscope (LSM 780, ZEISS). An excitation wavelength of 488 nm and emission range 500-530 nm were used for visualization the Mito-, ER- and Lyso-Tracker spots. For visualization of **4**, excitation at 543 nm and emission at 560-640 nm were used. The concentration of **4** was chosen to exclude any absorption of the dye in the green channel.

4.2.9 Caspases activity assays

The assays were performed with a caspase-3 colorimetric kit or caspase-8 and caspase-9 fluorimetric kits according to the manufacturer's protocol. Briefly, cells (1×10^6/well), seeded in 90 mm plates were incubated with **4** (2.5 μM) for 1 h followed by photo-illumination for 80 min, and the individual caspase activities were assayed at 16 h. The untreated but photo-exposed cells served as the control. Similar experiments were also carried out by pre-incubating the cells with the inhibitory peptides, Z-VAD-FMK, Z-IETD-FMK, Z-LEHD-FMK (each 20 μM), prior to other treatments.

4.2.10 Western blots

The whole cell extracts were prepared by lysing the **4** (0 or 2.5 μM)-treated and photo-exposed (80 min) A549 cells (1×10^6/well) in a lysis buffer (20 mM Tris (pH 7.4), 250 mM NaCl, 2 mM EDTA (pH 8.0), 0.1% Triton X-100, 0.01 μg/mL aprotinin, 0.01 μg/mL leupeptin, 0.4 mmol/L PMSF, and 4 mmol/L $NaVO_4$). The lysates were spun at 16500 × g for 10 min, the supernates collected and kept at -70 ^oC. The whole cell lysates (30 μg) were

separated by 12% SDS-polyacrylamide gel electrophoresis, and electrotransferred to nitrocellulose membrane. The membranes were blocked for 1 h at room temperature in TBST buffer (10 mM Tris–HCl, pH 8.0, 150 mM NaCl, and 0.1% Tween-20) containing 5% (w/v) nonfat milk, and then incubated overnight at 4 ^{o}C with the Caspase-3 specific primary antibody. After several washes, HRP-conjugated secondary antibody was added, the membranes were incubated further for 1 h, and the blots were developed using a Lumi-Light^{PLUS} western blotting kit. The bands were detected using a Kodak Gel-doc software and the intensity ratios of immunoblots to that of normal control, taken as 1 (arbitrary unit) were quantified after normalizing with respect to the loading controls.

4.3 Statistical analyses

The data were analyzed using a paired t test for the paired data or one way analysis of variance (ANOVA) followed by a Dunnet multiple comparisons post test. Values are expressed as means ± S.E.M. A probability value of $P<0.05$ was considered significant.

References

[1]. R. Bonnet, Chemical Aspects of Photodynamic Therapy; Gordon and Breach Science: Amsterdam, 2000.

[2]. T.J. Dougherty, An update on photodynamic therapy applications. J. Clin. Laser Med. Surg. 20 (2002) 3–7.

[3]. D.E. Dolmans, D. Fukumura, R.K. Jain, Photodynamic therapy for cancer. Nat. Rev. Cancer 3 (2003) 380–387.

[4]. P. Babilas, S. Schreml, M. Landthaler, R.M. Szeimies, Photodynamic therapy in dermatology: state-of-the-art. Photodermatol. Photoimmunol. Photomed. 26 (2010) 118–132.

[5]. S. Kossodo, G.M. LaMuraglia, Clinical potential of photodynamic therapy in cardiovascular disorders. Am. J. Cardiovasc. Drugs 1 (2001) 15–21.

[6]. G. Jori, Photodynamic therapy of microbial infections: state of the art and perspectives. J. Environ. Pathol. Toxicol. Oncol. 25 (2006) 505–519.

[7]. A.F. Cruess, G. Zlateva, A.M. Pleil, B. Wirostko, Photodynamic therapy with verteporfin in age-related macular degeneration: a systematic review of efficacy, safety, treatment modifications and pharmacoeconomic properties. Acta Ophthalmol. 87 (2009) 118–132.

[8]. M.A.M. Capella, L.S.J. Capella, A light in multidrug resistance: photodynamic treatment of multidrug-resistant tumors. J. Biomed. Sci. 10 (2003) 361–366.

[9]. B. Ballou, L.A. Ernst, A.S. Waggoner, Fluorescence imaging of tumors in vivo. Curr. Med. Chem. 12 (2005) 795–805.

[10]. W.M. Sharman, J.E. van Lier, C.M. Allen, Targeted photodynamic therapy via receptor mediated delivery systems. Adv. Drug Delivery Rev. 56 (2004) 53−76.

[11]. G. Zheng, H. Li, M. Zhang, S. Lund-Katz, B. Chance, J.D. Glickson, Low-density lipoprotein reconstituted by pyropheophorbide cholesteryl oleate as target-specific photosensitizer. Bioconjugate Chem. 13 (2002) 392−396.

[12]. S.B. Brown, E.A. Brown, I. Walker, The present and future role of photodynamic therapy in cancer treatment. Lancet Oncol. 5 (2004) 497–508.

[13]. R.R. Allison, G.H. Downie, R. Cuenca, X.H. Hu, C.J. Childs, C.H. Sibata, Photosensitizers in clinical PDT. Photodiagnosis Photodyn. Ther. 1 (2004) 27–42.

[14]. T. Hasan, B. Ortel, N. Solban, B.W. Pogue, Photodynamic therapy of cancer. In: D.W. Kufe, R. Bast, W. Hait, W.K. Hong, R.E. Pollock, R.R. Weichselbaurm, R.C. Bast, Jr., T.S. Gansler, J.F. Holland and E. Frei, III, editors. Cancer Medicine, 7th ed. Hamilton, Ontario, Canada: BC Decker, Inc.; 2006. p. 537–48.

[15]. A.E. O'Connor, W.M. Gallagher, A.T. Byrne, Porphyrin and nonporphyrin photosensitizers in oncology: preclinical and clinical advances in photodynamic therapy. Photochem. Photobiol. 85 (2009) 1053–1074.

[16]. G. Ulrich, R. Ziessel, A. Harriman, The chemistry of fluorescent bodipy dyes: Versatility unsurpassed. Angew. Chem. Int. Ed. 47 (2008) 1184–1201.

[17]. S.G. Awuah, Y. You, Boron dipyrromethene (BODIPY)-based photosensitizers for photodynamic therapy. RSC Adv. 2 (2012) 11169–11183.

[18]. A. Kamkaew, S.H. Lim, H.B. Lee, L.V. Kiew, L.Y. Chung, K. Burgess, BODIPY dyes in photodynamic therapy. Chem. Soc. Rev. 42 (2013) 77–88.

[19]. B.G. Davis, M.A. Robinson, Drug delivery systems based on sugar-macromolecule conjugates. Curr. Opin. Drug Discov. Develop. 5 (2002) 279–288.

[20]. X. Zheng, R.K. Pandey, Porphyrin-carbohydrate conjugates: impact of carbohydrate moieties in photodynamic therapy (PDT). Anticancer Agents Med. Chem. 8 (2008) 241–268.

[21]. E. Hao, T.J. Jensen, M.G. Vicente, Synthesis of porphyrin-carbohydrate conjugates using "click" chemistry and their preliminary evaluation in human HEp2 cells. J. Porph. Phthalo. 1 (2009) 51–59.

[22]. Y. Urano, D. Asanuma, Y. Hama, Y. Koyama, T. Barrett, M. Kamiya, T. Nagano, T. Watanabe, A. Hasegawa, P.L. Choyke, H. Kobayashi, Selective molecular imaging of viable cancer cells with pH-activatable fluorescence probes. Nat. Med. 15 (2009) 104–109.

[23]. A. Ojida, T. Sakamoto, M.a. Inoue, S.-h. Fujishima, G. Lippens, I. Hamachi, Fluorescent BODIPY-based Zn(II) complex as a molecular probe for selective detection of neurofibrillary tangles in the brains of Alzheimer's disease patients. J. Am. Chem. Soc. 131 (2009) 6543–6548.

[24]. M. Ono, H. Watanabe, H. Kimura, H. Saji, BODIPY-based molecular probe for imaging of cerebral β-amyloid plaques. ACS Chem. Neurosci. 3 (2012) 319–324.

[25]. S. Atilgan, Z. Ekmekci, A. L. Dogan, D. Guc, E. U. Akkaya, Water soluble distyryl-boradiazaindacenes as efficient photosensitizers for photodynamic therapy. Chem. Commun. 42 (2006) 4398–4400.

[26]. H. He, P.-C. Lo, S.-L. Yeung, W.-P. Fong, D.K.P. Ng, Synthesis and in vitro photodynamic activities of pegylated distyryl boron dipyrromethene derivatives. J. Med. Chem. 54 (2011) 3097–3102.

[27]. H. He, P.-C. Lo, S.-L. Yeung, W.-P. Fong, D.K.P. Ng, Preparation of unsymmetrical distyryl BODIPY derivatives and effects of the styryl substituents on their in vitro photodynamic properties. Chem. Commun. 47 (2011) 4748–4750.

[28]. T. Papalia, G. Siracusano, I. Colao, A. Barattucci, M.C. Aversa, S. Serroni, G. Zappal, S. Campagna, M.T. Sciortino, F. Puntoriero, P. Bonaccorsi, Cell internalization of

BODIPY-based fluorescent dyes bearing carbohydrate residues. Dyes and Pigments 110 (2014) 67–71.

[29]. M.L. Lepage, A. Mirloup, M. Ripoll, F. Stauffert, A. Bodlenner, R. Ziessel, P. Compain, Design, synthesis and photochemical properties of the first examples of iminosugar clusters based on fluorescent cores. Beilstein J. Org. Chem. 11 (2015) 659–667.

[30]. T. Uppal, N.V.S.D.K. Bhupathiraju, M.G.H. Vicente, Synthesis and cellular properties of Near-IR BODIPY‑PEG and carbohydrate conjugates. Tetrahedron 69 (2013) 4687–4693.

[31]. N. M. Gretskaya, V.V. Bezuglov, Synthesis of BODIPY® FL C5-labeled d-erythro and l-threo- lactosylceramides. Chem. Nat. Comp. 49 (2013) 17–20.

[32]. P. Bonaccorsi, M.C. Aversa, A. Barattucci, T. Papalia, F. Puntoriero, S. Campagna, Artificial light-harvesting antenna systems grafted on a carbohydrate platform. Chem. Commun. 48 (2012) 10550–10552.

[33]. B. Liu, N. Novikova, M.C. Simpson, M.S.M. Timmer, B.L. Stocker, T. Söhnel, D.C. Warea, P.J. Brothers, Lighting up sugars: fluorescent BODIPY–glucofuranose and –septanose conjugates linked by direct B–O–C bonds. Org. Biomol. Chem. DOI: 10.1039/c6ob00726k.

[34]. S. Mula, A.K. Ray, M. Banerjee, T. Chaudhuri, K. Dasgupta, S. Chattopadhyay, Design and development of a new pyrromethene dye with improved photostability and lasing efficiency: Theoretical rationalization of photophysical and photochemical properties. J. Org. Chem. 73 (2008) 2146–2154.

[35]. S. Mula, G. Ulrich, R. Ziessel, Bodipy fluorophores linked by polyethyleneglycol spacers. Tetrahedron Lett. 50 (2009) 6383–6388.

[36]. N. Shivran, S. Mula, T.K. Ghanty, S. Chattopadhyay, Steric strain release-directed regioselective functionalization of meso-methyl bodipy dyes. Org. Lett. 13 (2011) 5870–5873.

[37]. K.K. Jagtap, N. Shivran, S. Mula, D.B. Naik, S.K. Sarkar, T. Mukherjee, D.K. Maity, A.K. Ray, Change of boron substitution improves the lasing performance of bodipy dyes: A mechanistic rationalisation. Chem. Eur. J. 19 (2013) 702–708.

[38]. M. Gupta, S. Mula, M. Tyagi, T.K. Ghanty, S. Murudkar, A.K. Ray, S. Chattopadhyay, Rational design of boradiazaindacene (BODIPY)-based functional molecules. Chem. Eur. J. 19 (2013) 17766–17772.

[39]. Y. Cakmak, S. Kolemen, S. Duman, Y. Dede, Y. Dolen, B. Kilic, Z. Kostereli, L.T. Yildirim, A. Lale Dogan, D. Guc, E.U. Akkaya, Designing excited states: Theory-guided access to efficient photosensitizers for photodynamic action. Angew. Chem. Int. Ed. 50 (2011) 11937–11941.

[40]. S.H. Lim, C. Thivierge, P. Nowak-Sliwinska, J. Han, H. van den Bergh, G. Wagnieres, K. Burgess, H.B. Lee, In vitro and in vivo photocytotoxicity of boron dipyrromethene derivatives for photodynamic therapy. J. Med. Chem. 53 (2010) 2865–2874.

[41]. S.L. Yong, L. Xiaoqiong, Y. Rong, L. Source, X. Jinping, Chinese patent CN103755753, Apr 30, 2014.

[42]. A. Kamkaew and K. Burgess, Double-targeting using a TrkC ligand conjugated to dipyrrometheneboron difluoride (BODIPY) based photodynamic therapy (PDT) agent. J. Med. Chem. 56 (2013) 7608−7614.

[43]. A. Jemal, L.X. Clegg, E. Ward, L.A. Ries, X. Wu, P.M. Jamison, P.A. Wingo, H.L. Howe, R.N. Anderson, B.K. Edwards, Annual report to the nation on the status of cancer, 1975-2001, with a special feature regarding survival. Cancer 101 (2004) 3–27.

[44]. F. Kamangar, G.M. Dores, W.F. Anderson, Patterns of cancer incidence, mortality, and prevalence across five continents: defining priorities to reduce cancer disparities in different geographic regions of the world. J. Clin. Oncol. 24 (2006) 2137–2150.

[45]. S. Lam, Photodynamic therapy of lung cancer. Semin. Oncol. 21(6 Suppl 15) (1994) 15–19.

[46]. O. Buyukcakir, O. A. Bozdemir, S. Kolemen, S. Erbas and E. U. Akkaya, Tetrastyryl-bodipy dyes: Convenient synthesis and characterization of elusive near IR fluorophores. Org. Lett. 11 (2009) 4644–4647.

[47]. T. Bura, P. Retailleau, G. Ulrich, R. Ziessel, Highly substituted bodipy dyes with spectroscopic features sensitive to the environment. J. Org. Chem. 76 (2011) 1109–1117.

[48]. L. Six, K.-P. Rueβ, M. Liefänder, An efficient and stereoselective synthesis of 1,2-0-dialkyl-3-0-β-d-dlycosyl-sn-glycerols. Tetrahedron Lett. 24 (1983) 1229–1232.

[49]. A.F. Casy, PMR Spectroscopy in Medicinal and Biological Chemistry, Academic Press, London, 1971, pp. 330–384.

[50]. W. Rettig, Charge separation in excited states of decoupled systems—TICT compounds and implications regarding the development of new laser dyes and the primary processes of vision and photosynthesis. Angew. Chem., Int. Ed. 25 (1986) 971–988.

[51]. J.D. McGhee, P.H. von Hippel, Theoretical aspects of DNA protein interactions: cooperative and non cooperative binding of large ligands to a one dimensional homogeneous lattice. J. Mol. Biol. 86 (1974) 469–489.

[52]. W.D. Wilson, A.N. Gough, J.J. Doyle, Coralyne. Intercalation with DNA as a possible mechanism of antileukemic action. J. Med. Chem. 19 (1976) 1261–1263.

[53]. S.K. Pandey, X. Zheng, J. Morgan, J.R. Missert, T.-H. Liu, M. Shibata, D.A. Bellnier, A.R. Oseroff, B.W. Henderson, T.J. Dougherty, R.K. Pandey, Purpurinimide carbohydrate conjugates: Effect of the position of the carbohydrate moiety in photosensitizing efficacy. Mol. Pharmaceutics 4 (2007) 448-464.

[54]. S. Banfi, E. Caruso, S. Zaza, M. Mancini, M.B. Gariboldi, E. Monti, Synthesis and photodynamic activity of a panel of BODIPY dyes. J. Photochem. Photobiol. B: Biol. 114 (2012) 52–60.

[55]. N.N. Danial, S.J. Korsmeyer, Cell death: critical control points. Cell 116 (2004) 205–219.

[56]. A. Ashkenazi, V.M. Dixit, Death receptors: Signaling and modulation. Science 281 (1998) 1305–1308.

[57]. K.F. Ferri, G. Kroemer, Organelle-specific initiation of cell death pathways. Nat. Cell Biol. 3 (2001) 255–263.

[58]. N.L. Oleinick, R.L. Morris, I. Belichenko, The role of apoptosis in response to photodynamic therapy: What, where, why, and how. Photochem. Phtobiol. Sci. 1 (2002) 1–21.

[59]. G.-Y. Liou, P. Storz, Reactive oxygen species in cancer. Free Radic Res. 44 (2010) 479–496.

[60]. B. D'Autréaux, M.B. Toledano, ROS as signalling molecules: mechanisms that generate specificity in ROS homeostasis. Nat. Rev. Mol. Cell Biol. 8 (2007) 813–824.

[61]. S.P. Stratton, D.C. Liebler, Determination of singlet oxygen-specific versus radical-mediated lipid peroxidation in photosensitized oxidation of lipid bilayers: Effect of β-carotene and α-tocopherol. Biochem. 36 (1997) 12911–12920.

[62]. E. Buytaert, G. Callewaert, N. Hendrickx, L. Scorrano, D. Hartmann, L. Missiaen, J.R. Vandenheede, I. Heirman, J. Grooten, P. Agostinis, Role of endoplasmic

reticulum depletion and multidomain proapoptotic BAX and BAK proteins in shaping cell death after hypericin-mediated photodynamic therapy. FASEB J. 20 (2006) 756–758.

[63]. Y.J. Hsieh, C.C. Wu, C.J. Chang, J.S. Yu, Subcellular localization of Photofrin® determines the death phenotype of human epidermoid carcinoma A431 cells triggered by photodynamic therapy: When plasma membranes are the main targets. J. Cell. Physiol. 194 (2003) 363–375.

[64]. J. Saczko, M. Mazurkiewicz, A. Chwiłkowska, J. Kulbacka, G. Kramer, M. Ługowski, M. Śnietura, T. Banaś, Intracellular distribution of Photofrin® in malignant and normal endothelial cell lines. Folia Biologica (Praha) 53 (2007) 7–12.

[65]. A.L. Gryshuk, Y. Chen, W. Potter, T. Ohulchansky, A. Oseroff, R.K. Pandey, In vivo stability and photodynamic efficacy of fluorinated bacteriopurpurinimides derived from bacteriochlorophyll-a. J. Med. Chem. 49 (2006) 1874–1881.

[66]. K.Q. Luo, V.C. Yu, Y. Pu, D.C. Chang, Application of the fluorescence resonance energy transfer method for studying the dynamics of caspase-3 activation during UV-induced apoptosis in living HeLa cells. Biochem. Biophys. Res. Commun. 283 (2001) 1054–1060.

[67]. M. Mahitosh, M. Liana, K. Rakesh, Biochem. Redistribution of activated caspase-3 to the nucleus during butyric acid-induced apoptosis. Biophys. Res. Commun. 260 (1999) 775–780.

[68]. T. Kiwamu, N. Takeharu, M. Atsushi, M. Masayuki, Spatio-temporal activation of caspase revealed by indicator that is insensitive to environmental effects. J. Cell Biol. 160 (2003) 235–243.

[69]. R. Ezzeddine, A. Al-Banaw, A. Tovmasyan, J. D. Craik, I. Batinic-Haberle, L. T. Benov, Effect of molecular characteristics on cellular uptake, subcellular localization,

and phototoxicity of Zn(II) *N*-alkylpyridylporphyrins**.** J. Biol. Chem. 288 (2013) 36579–36588.

[70]. R. Leth-Larsen, R.R. Lund, H.J. Ditzel, Plasma membrane proteomics and its application in clinical cancer biomarker discovery. Mol. Cell Proteom. 9 (2010) 1369–1382.

[71]. A. Gomes, E. Fernandes, J.L.F.C. Lima, Fluorescence probes used for detection of reactive oxygen species. J. Biochem. Biophys. Methods 65 (2005) 45–80.

[72]. T. Mosmann, Rapid colorimetric assay for cellular growth and survival: application to proliferation and cytotoxicity assays. J. Immunol. Meth. 65 (1983) 55–63.

[73]. http://www.flowjo.com/v6/html/faq.html#2.7.2

Figure legends

Fig. 1. Chemical structures of the test BODIPYs.

Fig. 2. Amongst the test BODIPYs, dye 4 shows the best PDT property against the human lung cancer A549 cell line. A: Dose-dependent cytotoxicities of the test BODIPYs. The A549 cells (1×10^4/well) were treated with vehicle (0.1% DMSO) or increasing concentrations of the test compounds for 1 h, followed by photo-exposure (irradiance: 0.77 mW/cm^2) for 80 min. The cell viability at 24 h was assessed by the MTT assay. Results are expressed in percentage considering that of the untreated control cells as 100. **B:** Detection of necrosis. **i:** vehicle-treated cells, **ii-iv:** cells treated with **1**, **4** and **6** (each 2.5 μM) respectively. The A549 cells (1×10^5 cells/well) were treated as above. After 2 h, the washed cells were stained with trypan blue, examined, and photographed with a microscope. The experiments were repeated three times with similar results. All determinations were made in five replicates and the values are mean ± S.E.M. $^{*}p<0.05$, $^{**}p<0.01$, $^{***}p<0.001$ compared to vehicle control. Representative images are shown.

Fig. 3. BODIPY 4 induces apoptosis in A549 cells on photo-irradiation. A and **B:** Histogram and quantification of the sub-G1 cell population analyses. **i-iii:** photo-exposure period 0 min, 30 min and 80 min respectively. The A549 cells were incubated with vehicle (0.1% DMSO) or **4** (5-50 μM) for 1 h, followed by photo-exposure (irradiance: 0.77 mW/cm^2) for different periods. The sub-G1 populations were analyzed by flow cytometry. **C:** Alteration of A549 cells morphology. **i:** control cells, **ii-iv:** cells treated with **4** (0.625, 1.25 and 2.5 μM) respectively followed by photo-exposure for 80 min. The A549 cells were treated with vehicle or different concentrations of **4** for 1 h, followed by photo-exposure for 80 min. After incubating the cells in a regular medium for 24 h, the cells were visualized under a phase contrast microscope. The experiments were repeated three times with similar results. All determinations were made in five replicates and the values are means ± S. E. M.

$^{*}p<0.01$, $^{**}p<0.001$ compared to vehicle control. Representative images are shown. Arrows indicate apoptotic cells.

Fig. 4. BODIPY 4 activates caspase-8 and caspase-3, but not caspase-9 in A549 cells on photo-irradiation. A: Activation of the caspases. **B:** Effect of specific and pan caspase inhibitors on the PDT property of **4**. **C:** Immunoblots of caspase-3. The A549 cells as such or pre-incubated with specific caspase-3, caspase-8 and caspase-9 inhibitors (each 20 μM) for 1 h were incubated further with **4** (0 or 2.5 μM) for 1 h, followed by photo-exposure (irradiance: 0.77 mW/cm^2) for 80 min. The cell viability at 24 h was assessed by the MTT assay, while the activities of the caspases in the whole cell extracts were assayed after 16 h. The immunobloting was carried out with the whole cell extracts using the antibody against caspase-3. The protein bands were detected using a Kodak Gel-doc software and the intensity ratios of immunoblots to that of normal control, taken as 1 (arbitrary unit) were quantified after normalizing with respective loading controls. The experiments were repeated three times with similar results. All determinations were made in five replicates and the values are means ± S. E. M. $^{*}p<0.05$, $^{**}p<0.01$, $^{***}p<0.001$ compared to vehicle control; $^{\tau}p<0.05$, $^{\#}p<0.01$ compared to only **4**-treatment. Representative images are shown.

Fig. 5. Intracellular ROS is involved in the BODIPY 4-induced apoptosis in A549 cells on photo-irradiation. Effect of the ROS-scavengers, NAC (**A**) and β-carotene (**B**) on sub-G1 population. The A549 cells were incubated with **4** (0 or 2.5 μM) as such or in conjunction with NAC (5 mM) or β-carotene (50 and 100 μM) for 1 h, followed by photo-exposure (irradiance: 0.77 mW/cm^2) for 80 min. The sub-G1 populations were analyzed by flow cytometry. **C:** Dose-dependent effect of β-carotene on the photo-cytotoxicity of **4**. The cells were incubated with **4** (0 or 2.5 μM) in conjunction with β-carotene (0-100 μM) for 1 h as above, followed by photo-exposure. The cell viability at 24 h was assessed by the MTT assay. The experiments were repeated three times with similar results. All determinations

were made in five replicates and the values are means ± S. E. M. $^{*}p<0.001$ compared to control; $^{\tau}p<0.05$, $^{\#}p<0.01$ compared to only **4**-treatment. Representative histograms are shown.

Fig. 6. Uptake of the BODIPYs in A549 cells. A. Cells treated with **PM567** and dyes **1** and **2**. **B:** Cells treated with dyes **3-6**. The cells were incubated with the BODIPYs (1 μM) or Hoechst 33342 (10 μM) for different periods and the images captured with a fluorescence microscope. While overlaying the images, some minor adjustments to the stretch and tone of both blue and red images were made. The experiments were repeated three times with similar results. Representative images at 0.5 h are shown.

Fig. 7. Subcellular localization of dye 4 in A549 cells. Cells were treated with dye **4** (100 nM) for 1 h, followed by Lyso-Tracker Green (500 nM), Mito-Tracker Green (100 nM), or ER-Tracker Green (500 nM) for 0.5 h, washed and the images captured with a confocal microscope. Overlaying was done with the help of the ZEN-2012 (software). The experiments were repeated three times with similar results. Representative images at 0.5 h (magnification 63 ×, 1.4-NA oil objective) are shown.

Fig. 1

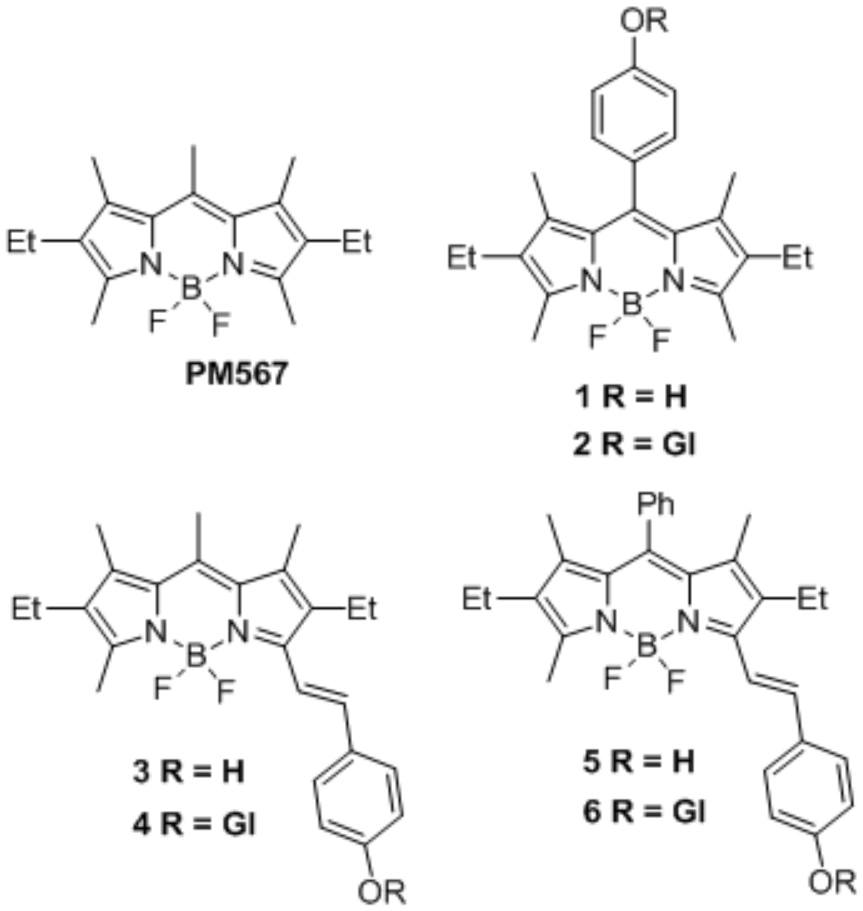

Fig. 2A

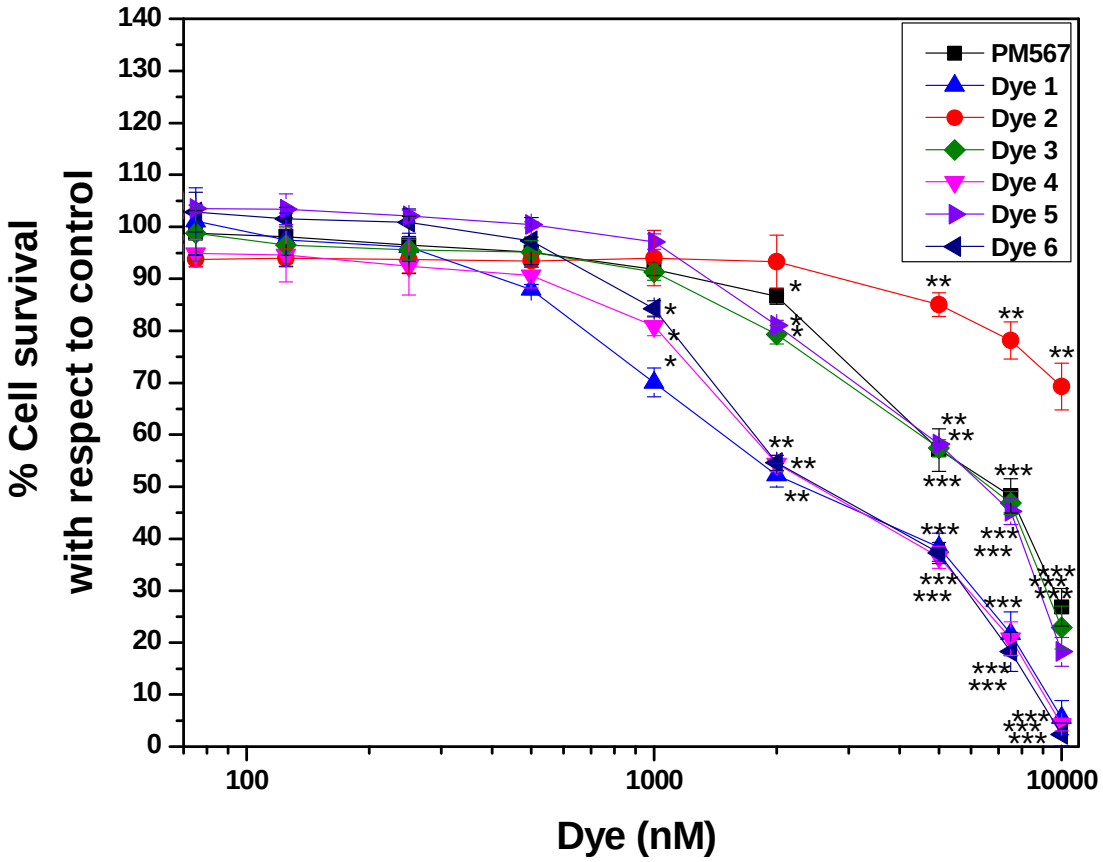
% Cell survival
with respect to control
Dye (nM)
PM567
Dye 1
Dye 2
Dye 3
Dye 4
Dye 5
Dye 6
0
10
20
30
40
50
60
70
80
90
100
110
120
130
140
100
1000
10000

Fig. 2B

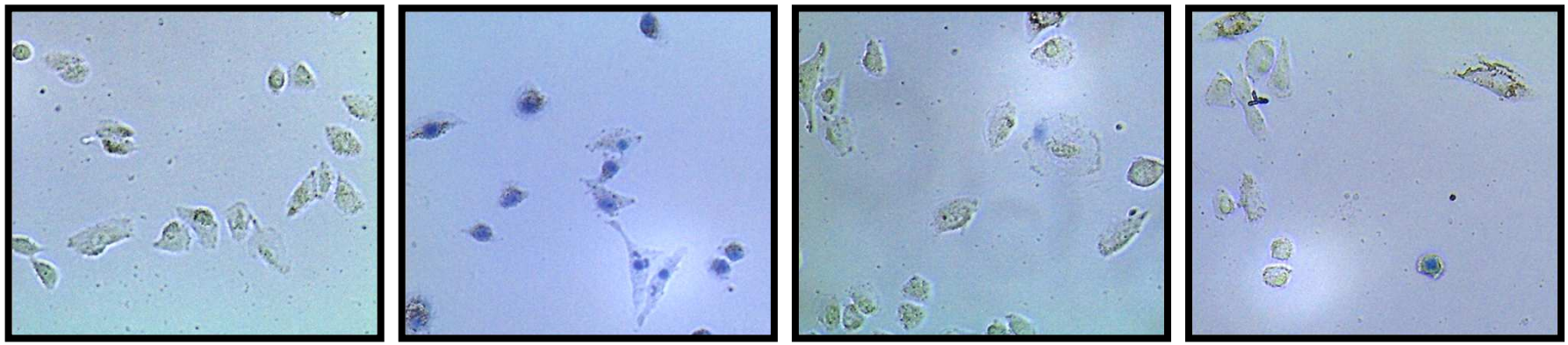

(i) (ii) (iii) (iv)

Fig. 3A

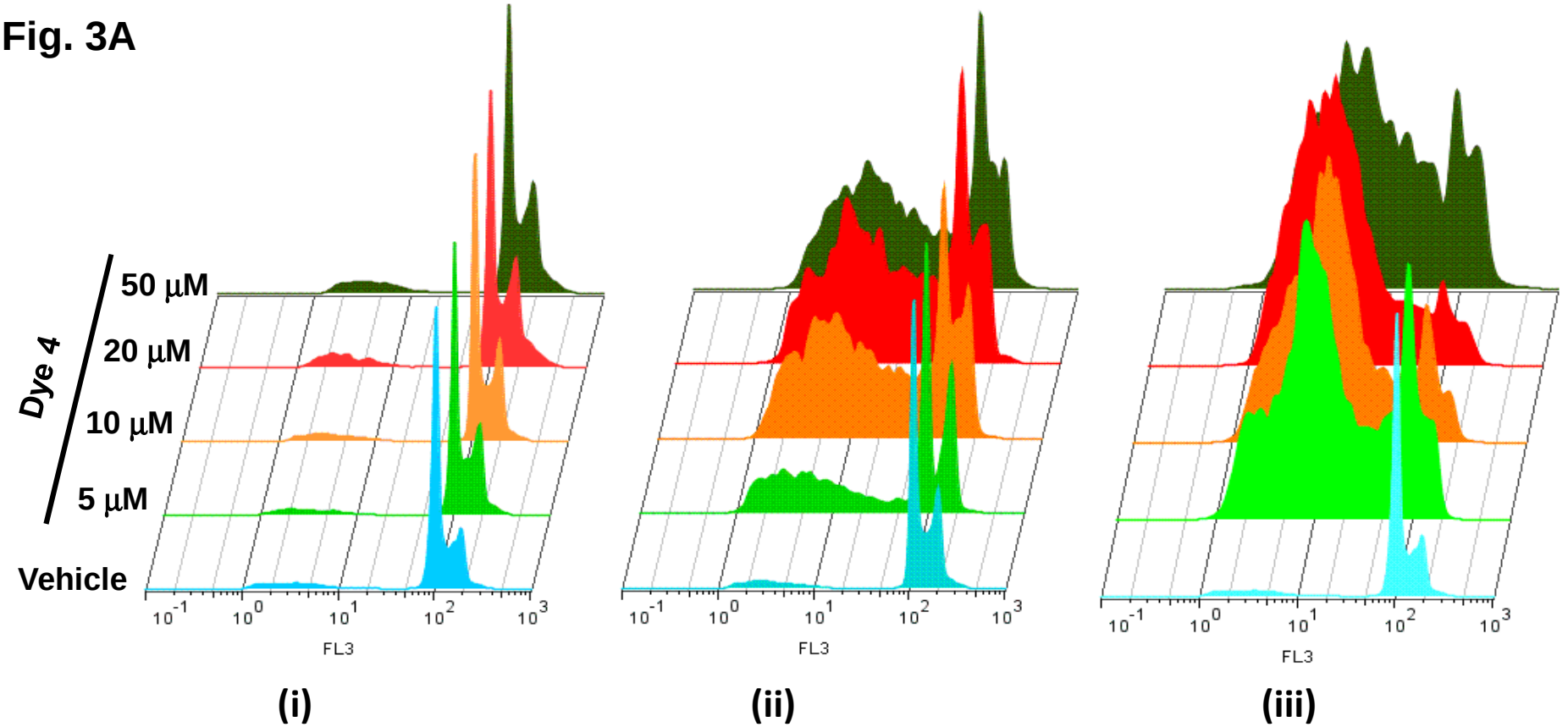

Fig. 3B

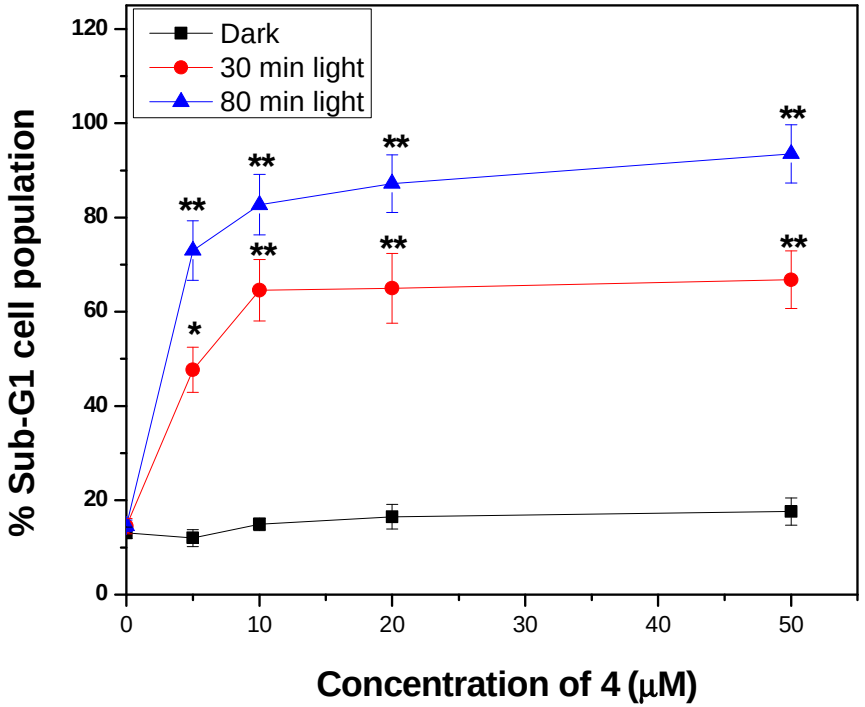
Dark
30 min light
80 min light
% Sub-G1 cell population
Concentration of 4 (μM)
0
20
40
60
80
100
120
0
10
20
30
40
50
*
**

Fig. 3C

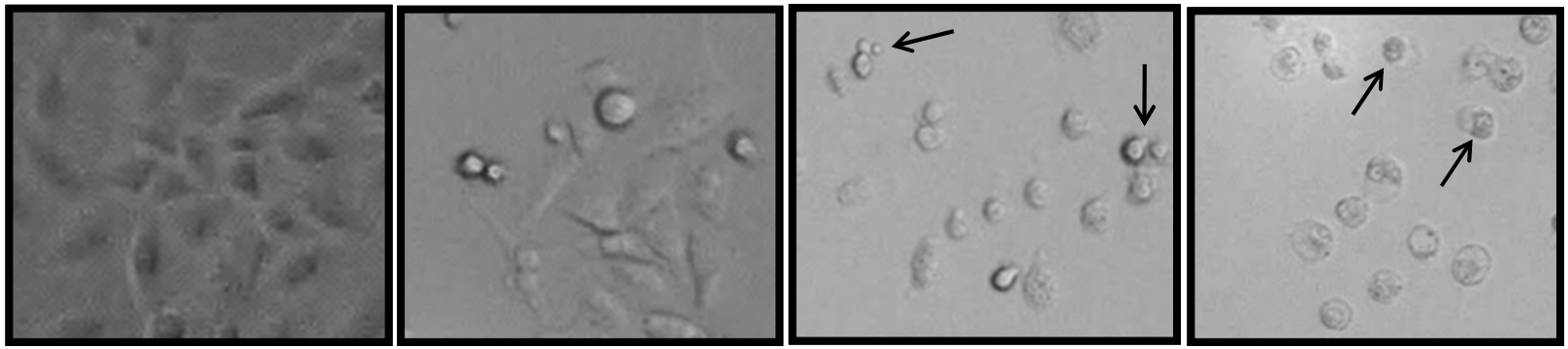

(i) (ii) (iii) (iv)

Fig. 4A

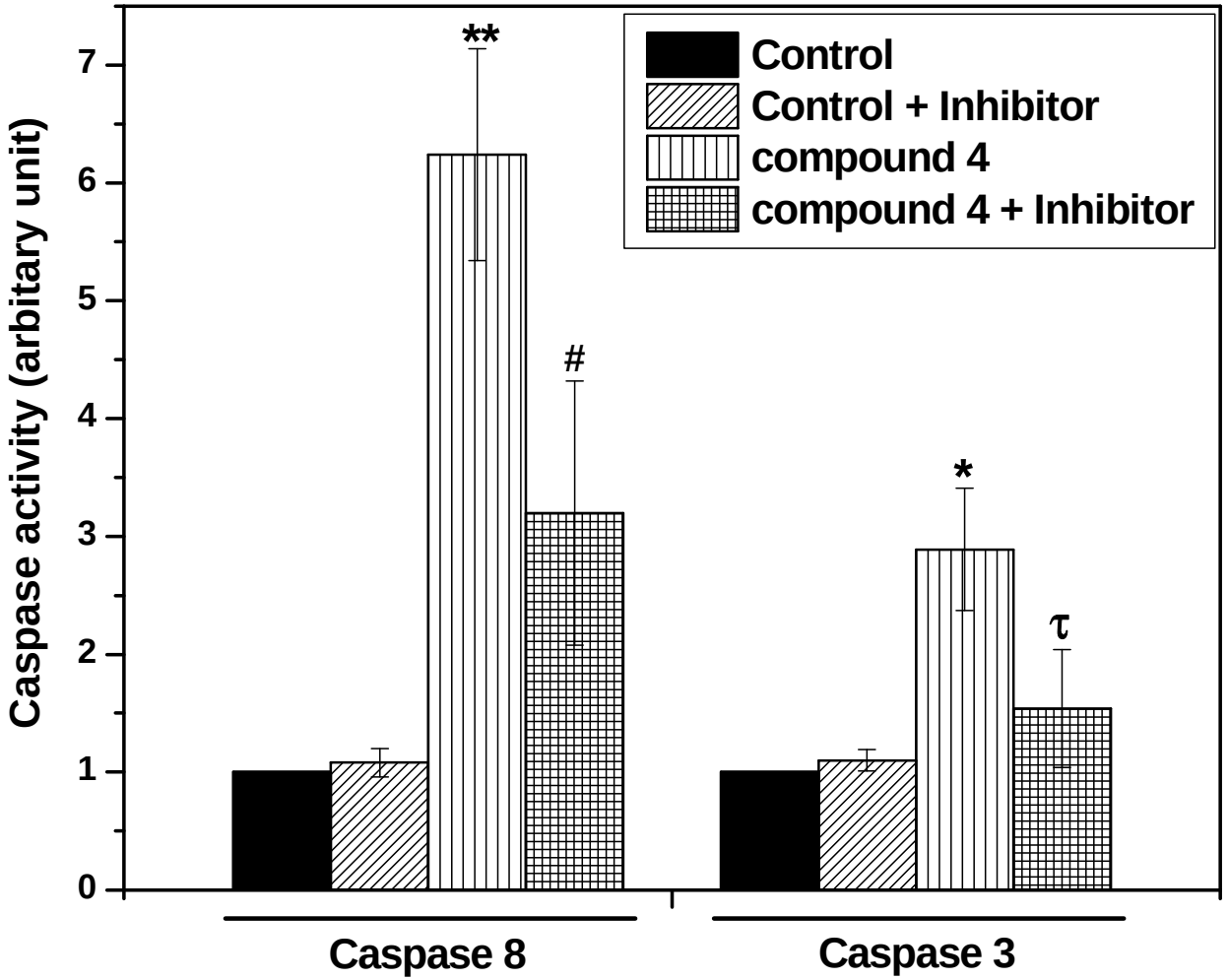

Fig. 4B

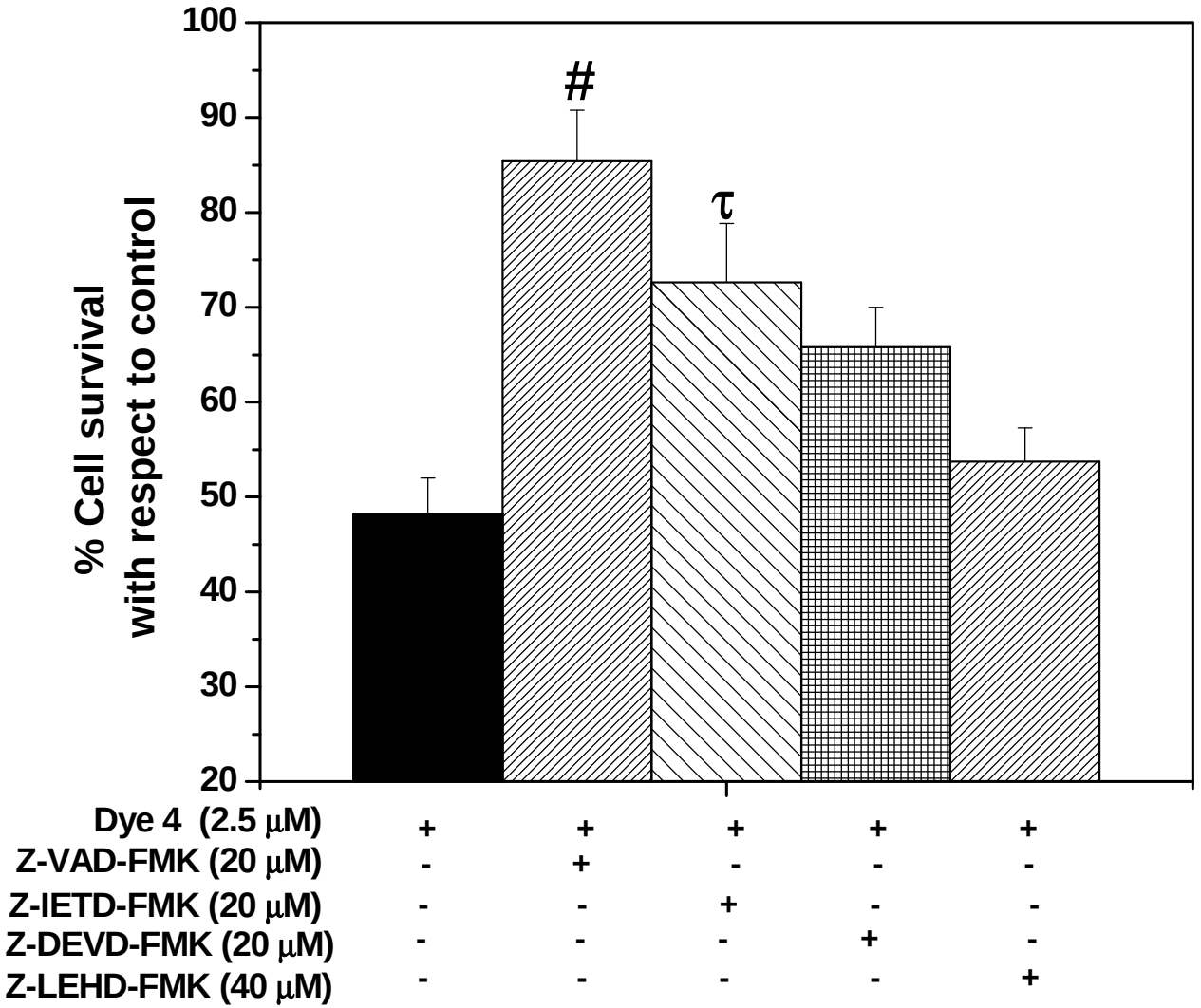

Fig. 4C

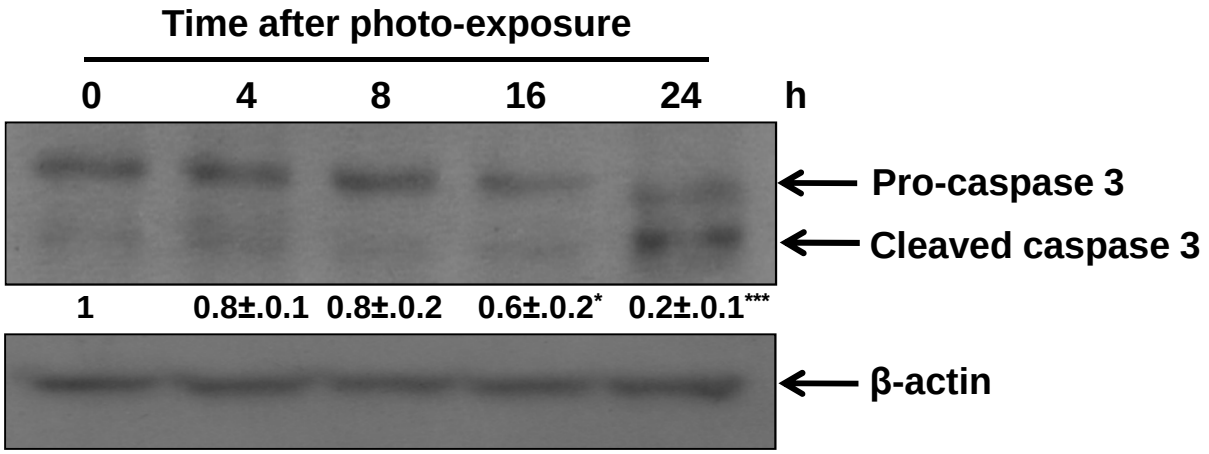

Fig. 5A

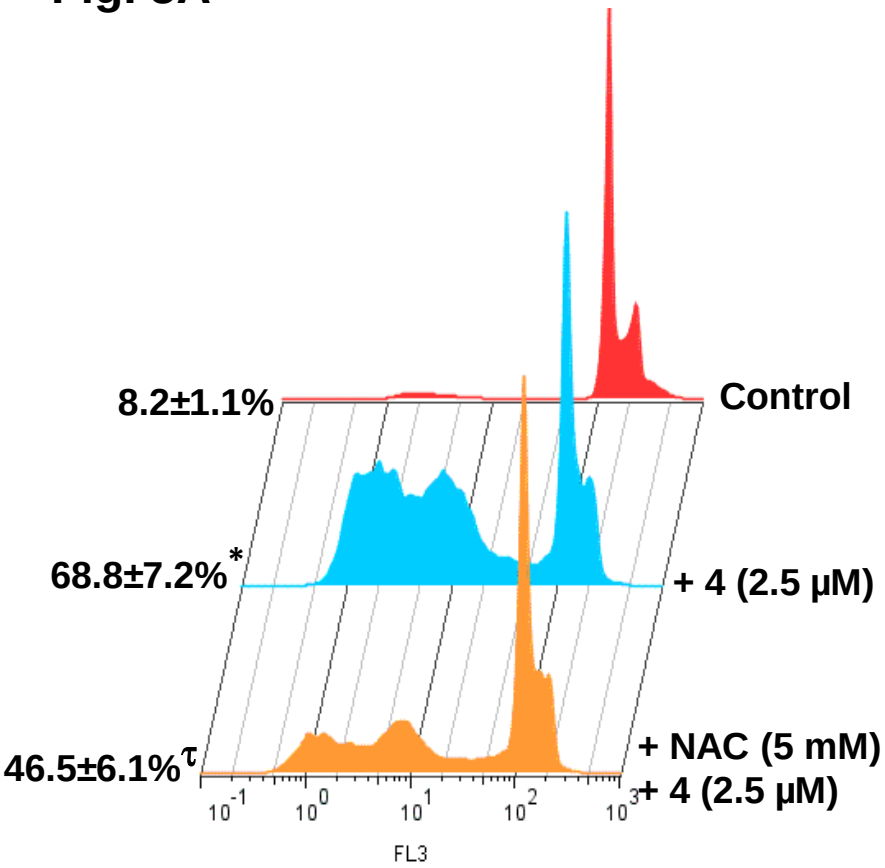

Fig. 5B

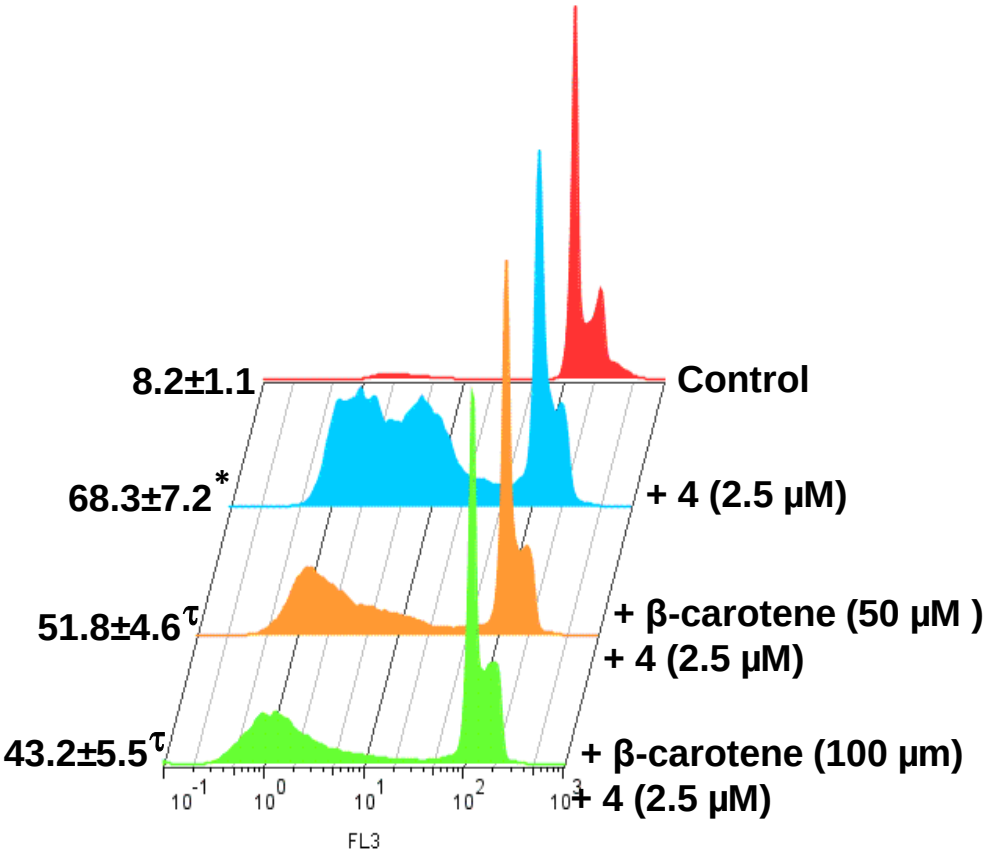

Fig. 5C

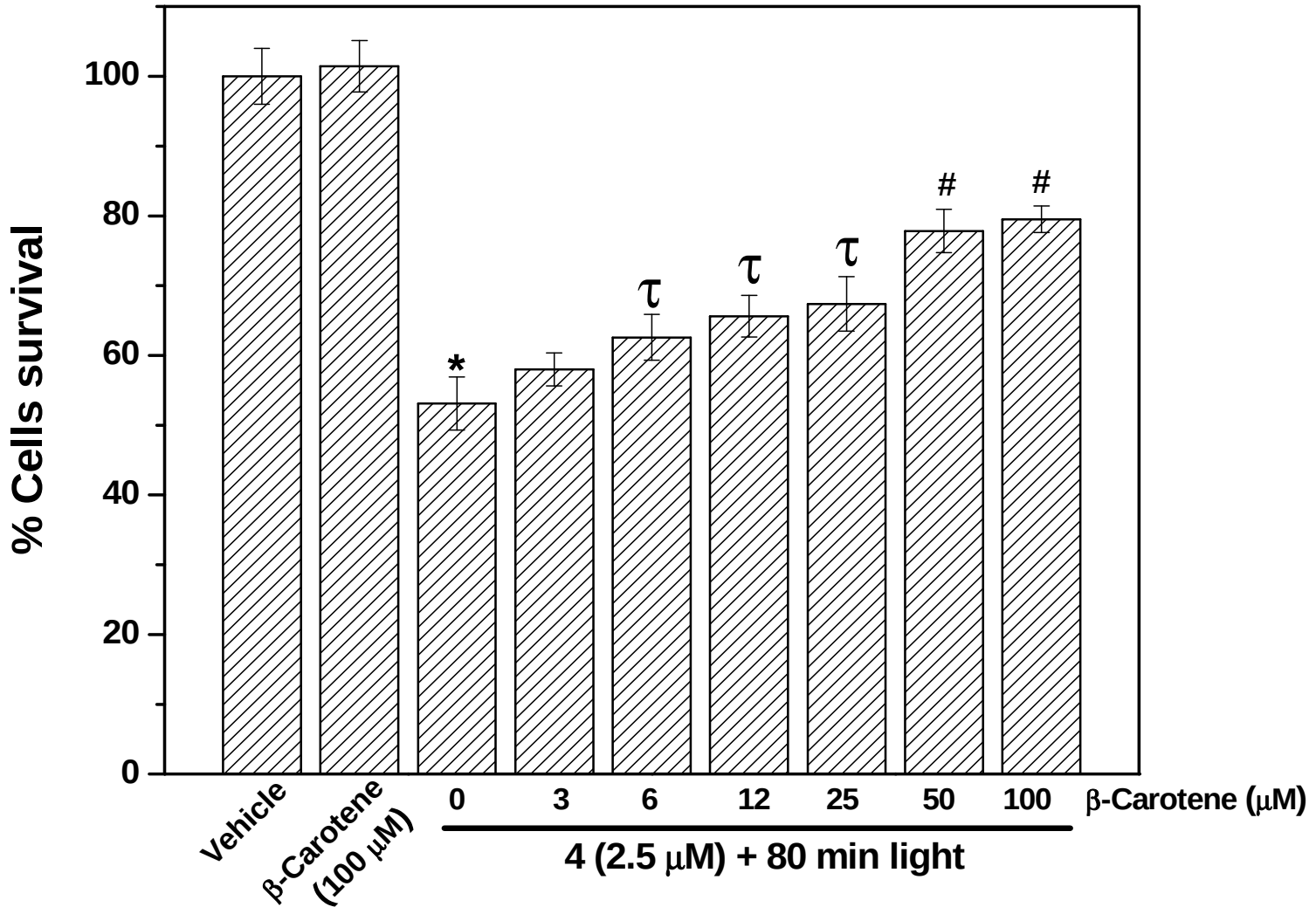

Fig. 6A

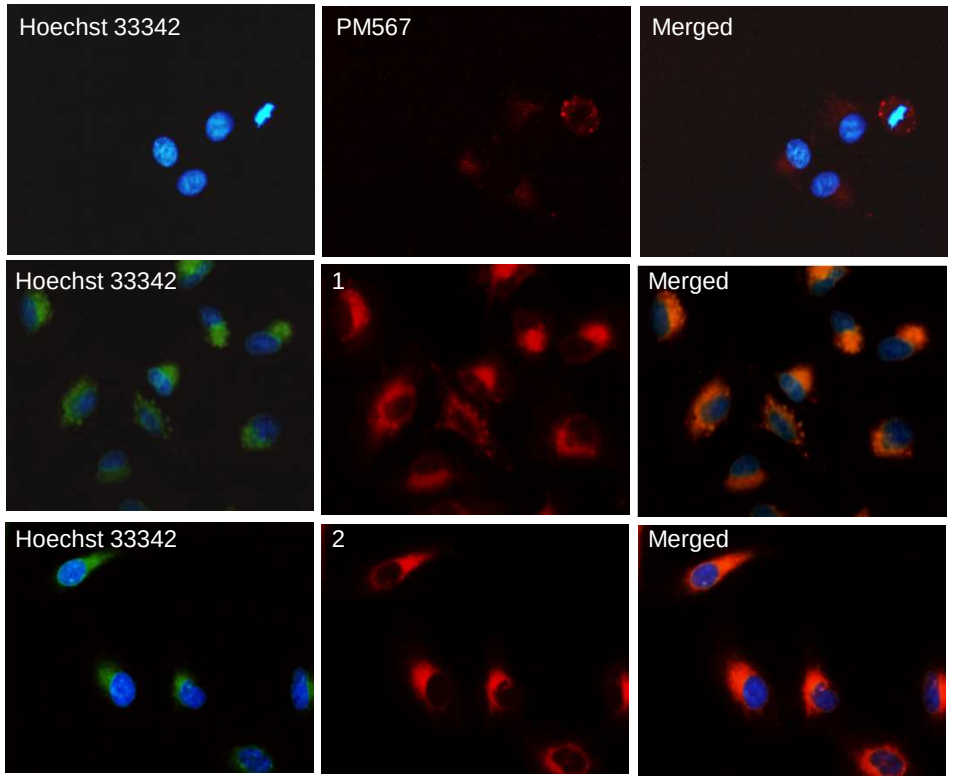
Hoechst 33342
PM567
Merged
Hoechst 33342
1
Merged
Hoechst 33342
2
Merged

Fig. 6B

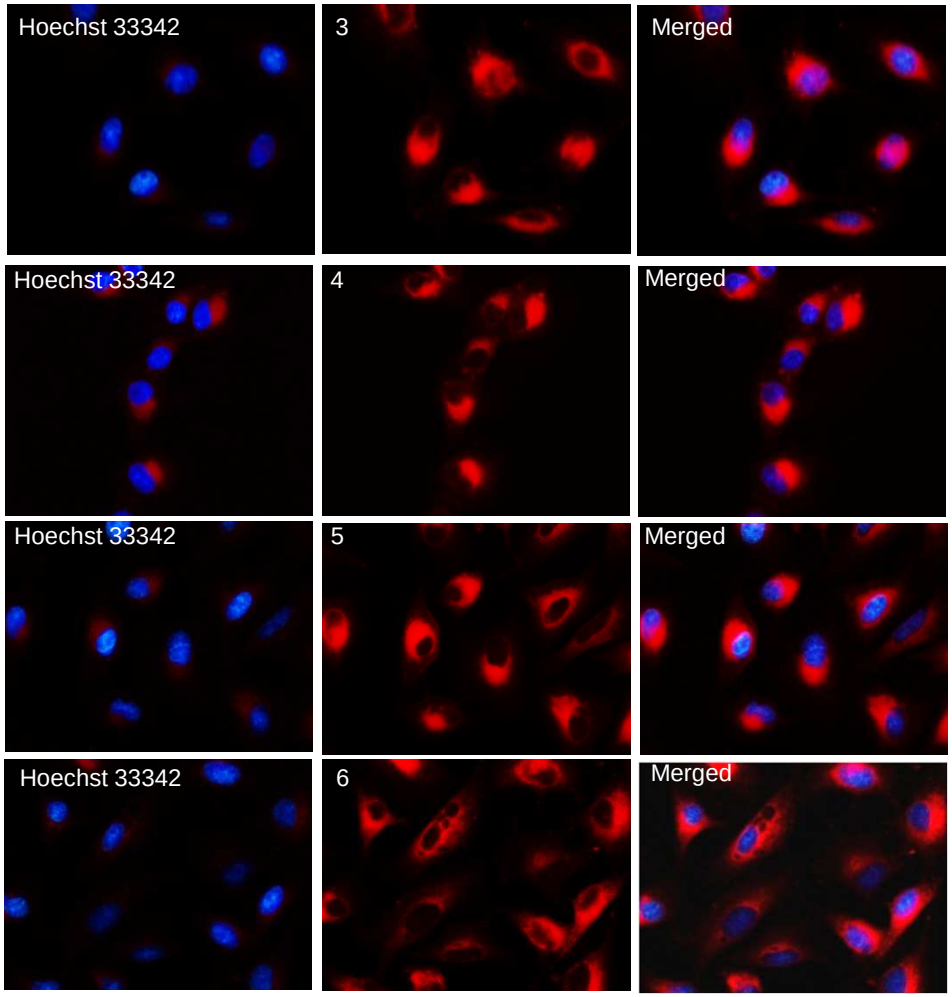
Hoechst 33342
3
Merged
Hoechst 33342
4
Merged
Hoechst 33342
5
Merged
Hoechst 33342
6
Merged

Fig. 7

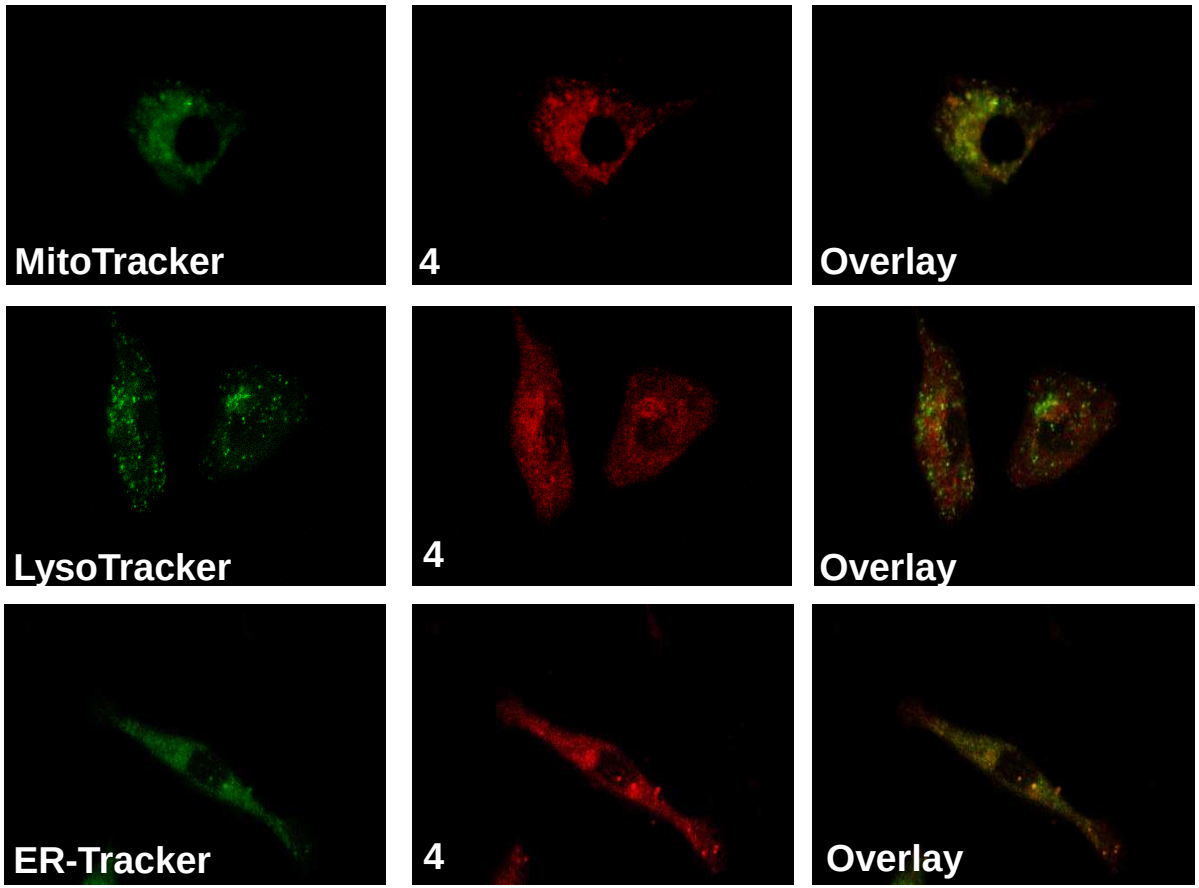
MitoTracker
4
Overlay
LysoTracker
4
Overlay
ER-Tracker
4
Overlay